GEM TN-93-316

GEM Noble Liquid Calorimeter Thermal Design Concept

May 26, 1993

Abstract:

Design concepts proposed for the cryogenics cooling system internal to the GEM detector are described and preliminary estimates of calorimeter heat loads, coolant flow rates, and heat exchanger performance are provided. Geometrics of the various heat exchangers and coolant supply and return manifolds are also described.

TN-93-316

GEM NOBLE LIQUID CALORIMETER THERMAL DESIGN CONCEPT

ABSTRACT

Design concepts proposed for the cryogenic cooling system internal to the GEM detector are described and preliminary estimates of calorimeter heat loads, coolant flow rates, and heat exchanger performance are provided. Geometries of the various heat exchangers and coolant supply and return manifolds are also described.

MAY 26, 1993

CONTENTS

1.0 INTRODUCTION 1

2.0 THERMAL DESIGN REQUIREMENTS 2
- 2.1 Barrel Calorimeter Requirements 4
- 2.2 End Cap Calorimeter Requirements 8

3.0 THERMAL DESIGN CONCEPT 10
- 3.1 Internal Cooling Circuits 11
  - 3.1.1 Barrel Calorimeter Cooling Circuits. 12
  - 3.1.2 End Cap Calorimeter Cooling Circuits 21
- 3.2 Feedthroughs 25
- 3.3 Support Stanchions 31
- 3.4 Thermal Bumpers 33
- 3.5 Super Insulation 33

4.0 CONTROL AND MONITORING SYSTEM 35
- 4.1 Temperature Sensors 35
- 4.2 Automatic Valves 35
- 4.3 Pressure Monitors 35
- 4.4 Flow Control and Monitoring 36

5.0 FUTURE WORK 36
- 5.1 System Reliability Trades 36
- 5.2 Three Dimensional Thermal Fluid Analysis 36
- 5.3 Thermo-Structural Analysis 37
- 5.4 Piping Feedthrough Design 37

6.0 REFERENCES 38

APPENDIX A A1

FIGURES

1-1 Cross -Sectional Views of the GEM Calorimeter (1/4 Model) 1
2-1 Schematic Diagram of the Calorimeter Coolant Conditioning Systems..... 3
2.1-1 Typical Barrel Calorimeter Hadronic Module. 5
2.1-2 Typical Barrel Calorimeter EM Module. 5
2.1-3 Barrel EM Module Cooling Loop & Circuit Board (A-N) Locations 6
2.2-1 Typical End Cap Calorimeter Hadronic Module. 8
2.2-2 End Cap Calorimeter EM Section. 9
3.1.1-1 Barrel Calorimeter Cooling Line and Manifold Piping Sizes. 13
3.1.1-2 Flow Diagram For The Barrel Calorimeter Cooling Circuit. 14
3.1.1-3 Internal End View of Barrel Calorimeter Showing Cooling Circuit Pipe Routes. 16
3.1.1-4 External End View of Barrel Calorimeter Showing the Routing of Utility and Instrumentation Lines. 17
3.1.1-5 Barrel Hadronic and Outer Liquid Vessel Cooling Lines. 18
3.1.1-6 Barrel Calorimeter Vacuum and LKr Supply Line Routes. 19
3.1.2-1 Top View of End Cap Calorimeter Showing Proposed EM Heat Exchanger Locations 22
3.1.2-2 Preliminary Cooling Circuit Routes for the End Cap Calorimeter 22
3.1.2-3 End Cap Calorimeter Vacuum and LAr Supply Routes. 24
3.2-1 View of Barrel Calorimeter Signal Cable Feedthrough Showing the Associated Cooling Circuit Layouts. 27
3.2-2 Barrel Calorimeter Outer EM Supply and Return Manifold Cold Feedthrough Concept. 28
3.2-3 Barrel Calorimeter LKr Supply Line and Vacuum Port Details. 29
3.2-4 End Cap Signal Cable Feedthrough and Associated Cooling Lines. 30
3.2-5 End Cap LAr Supply Line and Vacuum Port Details. 31
3.3-1 Typical GEM Calorimeter Support Stanchion With Thermal Intercept Details.. 32
3.5-1 Stackup of Minimum Allocated Space for the Placement of MLI. 34

TABLES

2-1 Summary of Calorimeter Heat Loads. 3

2.1-1 Barrel Calorimeter Segmentation and Channel Count. 4

2.1-2 Barrel EM Circuit Board Power Dissipation. 6

2.1-3 Barrel Calorimeter Heat Loads. 7

2.2-1 End Cap Calorimeter Segmentation and Channel Count. 9

2.2-2 Heat Loads for One End Cap Calorimeter. 10

3-1 Thermophysical Properties of Liquid Argon and Liquid Krypton. 11

3.1.1-1 LAr Coolant Flow Rates Associated With the Barrel Calorimeter Heat Loads Listed in Table 2.1-3. 13

3.1.1-2 Summary of Barrel Calorimeter Heat Exchanger Design Results. 20

3.1.2-1 LN2 Flow Rates Associated With The End Cap Heat Loads Listed In Table 2.2-1 23

1.0 INTRODUCTION

The GEM noble liquid calorimeter (Fig. 1-1) includes three large cryostats, the barrel and two end caps, containing liquid krypton (LKr) and liquid argon (LAr), respectively. These cryostats house and support electromagnetic (EM) and hadronic modules, the active elements of the calorimeter which constitute major internal sources of thermal energy. The cryostats are designed to achieve thermal balance within the cryogenic ionization media by:

1. Passively minimizing the thermal energy transmitted to the cryogenic fluids by conduction and radiation from external sources,

2. Actively intercepting thermal energy to preclude transmission to the ionization medium, and

3. Actively removing all thermal energy transmitted to the cryogenic fluids from both external and internal sources.

This report documents the barrel and end cap **internal** thermal control system design concepts in support of the GEM Technical Design Report (Ref. 1).

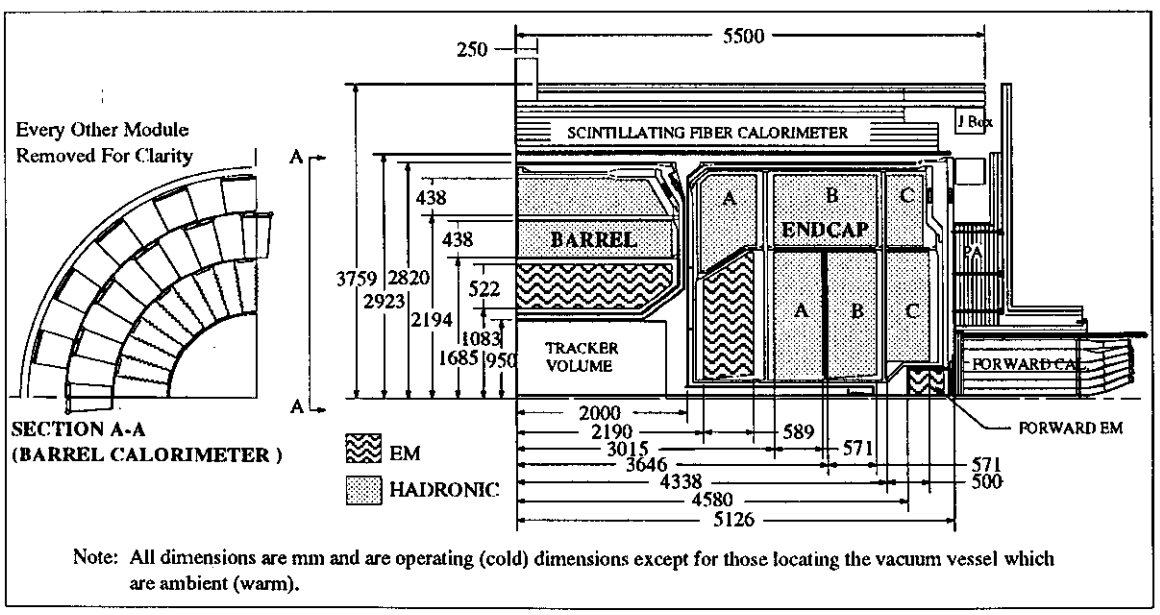

Note: All dimensions are mm and are operating (cold) dimensions except for those locating the vacuum vessel which are ambient (warm).

Figure 1-1 Cross -Sectional Views of the GEM Calorimeter (1/4 Model)

2.0 THERMAL DESIGN REQUIREMENTS

In achieving thermal balance, the cryostats and internal thermal control system must be designed to:

a) prevent localized boiling of the ionization medium and maintain the internal barrel and end cap cryostat temperatures at a uniform 120 ± 3 K and 87 ± 3 K respectively, and

b) insure that density fluctuations within the liquid cryogen ionization media are kept uniform to within 1.0% throughout the calorimeter sensing elements.

Although these two requirements are not strictly independent of one another, it is generally accepted that the first will drive the placement and size of cooling loops, while the second will define the particular heat exchanger geometry needed to meet the overall system stability requirements (i.e., monitoring, control, and flow balance requirements).

The net thermal energy which must be actively removed from the ionization media is a function of the effectiveness of the passive thermal control system and the level of internally generated thermal energy such as that dissipated by electronics. The passive elements of the thermal control system include the vacuum vessel, which provides an insulating vacuum, and multilayer insulation (MLI) both of which surround the cold liquid vessel. The insulating vacuum minimizes conduction while the MLI, which is located within the vacuum space, reduces thermal radiation transmitted to the cold vessel from the room temperature vacuum vessel. The derived requirements presented in the following sections assume the presence of these passive elements.

Other sources of thermal energy transmitted to the cryostat interiors include conduction via the vessel support stanchions and the various feedthroughs for cables and services.
A summary of the heat loads that the calorimeter cooling system must mitigate are provided in Table 2-1. Values corresponding to three levels of insulating vacuum are provided together with the amount of LN_2 usage required, assuming LN_2 boilers are employed as the final method of heat exchange with the ambient environment. Figure 2-1 depicts the separate closed recovery systems that are envisaged for the barrel and end cap cooling supplies. This report presents details of the GEM detector cryogenic cooling system that are **internal** to the calorimeter.

Table 2-1 Summary of Calorimeter Heat Loads.

	Heat Loads (Watts)		
Insulating Vacuum	**1.0 E-6 torr**	**4.0 E-4 torr**	**No Vacuum**
Barrel Calorimeter	10945	10971	19343
2 End Caps	10109	10151	30545
Totals (Watts)	**21054**	**21123**	**49888**
LN_2 Usage (l/day)	10460	10494	24784

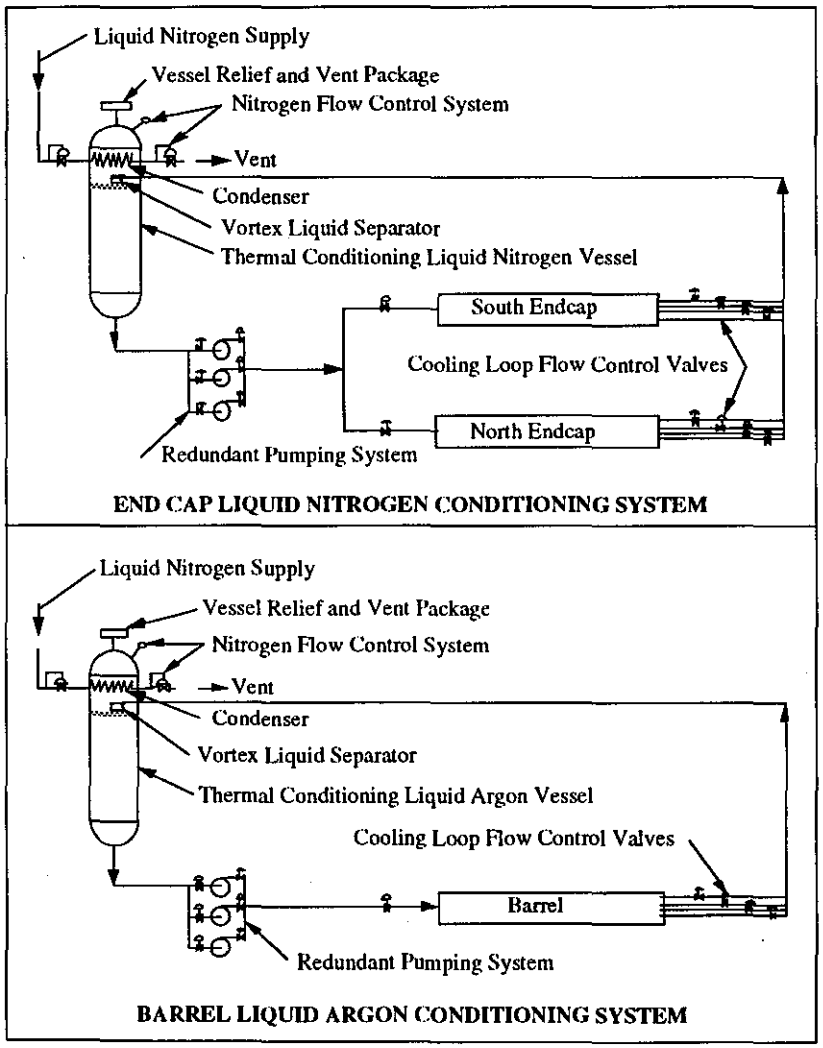

Figure 2-1 Schematic Diagram of the Calorimeter Coolant Conditioning Systems.

2.1 Barrel Calorimeter Requirements

The EM and hadronic modules within the barrel calorimeter are distributed as shown in Figure 1-1. The circumferential distribution of these modules and the number of associated data channels is identified in Table 2.1-1. Typical barrel hadronic and EM modules with the location of motherboards and cables are illustrated in Figures 2.1-1 and 2.1-2, respectively.

The EM section of the barrel calorimeter contains the highest concentration of electronics and requires the highest level of cooling and control. Each barrel EM module has 1,440 preamplifiers, with 960 mounted on the outer radius and 480 mounted on the inside radius. There are 80 towers in η and although they have the same number of preamplifiers they do not have the same power density distribution, because the circuit boards near the barrel center are physically smaller than those at the ends. This permits them to fit between the unevenly spaced outer circumferential tension band raceways (Ref. 2). Figure 2.1-3 and Table 2.1-2 show the power density distribution for a barrel EM module.

The hadronic section of the barrel calorimeter consists of two concentric rings of modules arranged as shown in Figure 1-1 and Table 2.1-1. The inner and outer rings, which have 160 modules each, represent 3,856 and 1,456 channels of data respectively. The nature of the hadronic module structure is such that the preamplifiers can be distributed more or less uniformly along their outer circumference resulting in average power densities of 6.0 W/m^2 for the inner modules and 2.0 W/m^2 for the outer modules.

The similarity between the GEM calorimeter support legs and those of the DØ detector suggests that for initial analyses a similar total heat leak of 41 watts/100 Mg of dead load can be assumed, resulting in a total of 191 W for the barrel supports (Ref. 3).

Table 2.1-1 Barrel Calorimeter Segmentation and Channel Count.

COMPONENT	SEGMENTATION $\eta \times \phi$ (x longitudinal)	No. OF MODULES in ϕ	No. OF CHANNELS
BARREL			
EM	.026 x .026 (x 3)	40	57,600
INNER HADRONIC	.078 x .078 (x 1)	80	3,856
OUTER HADRONIC	.078 x .078 (x 1)	80	1,456

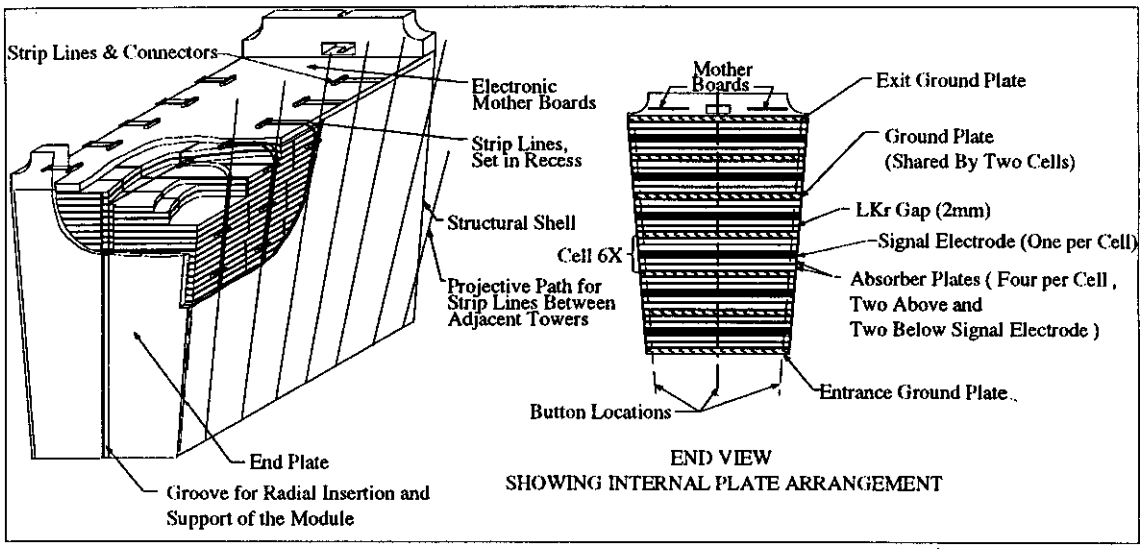

Figure 2.1-1 Typical Barrel Calorimeter Hadronic Module.

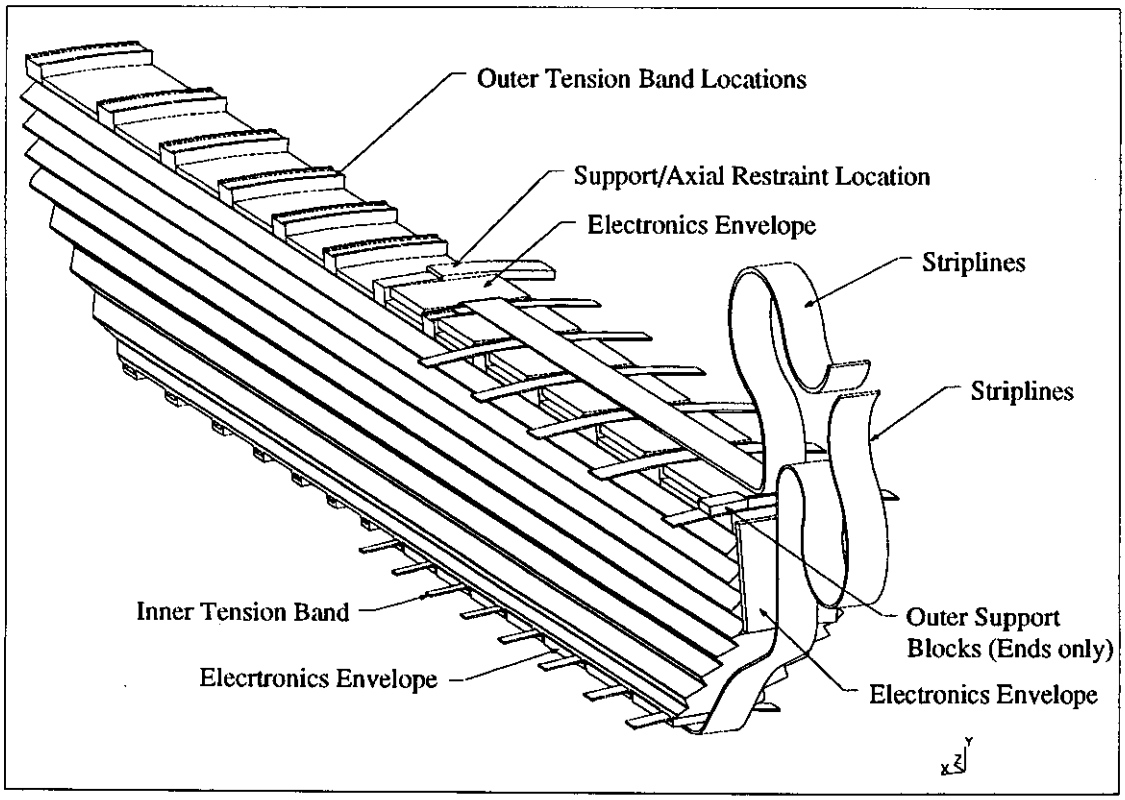

Figure 2.1-2 Typical Barrel Calorimeter EM Module.

Table 2.1-2 Barrel EM Circuit Board Power Dissipation.

CIRCUIT BOARD LOCATION*	RADIUS (mm)	Δ Z (mm)	AREA per MODULE (m^2)	POWER DISSIPATION (W/m^2)
A	1652	196.1	5.09E-02	1.35E+02
B	1652	197.6	5.13E-02	1.34E+02
C	1652	205.7	5.34E-02	1.28E+02
D	1652	220.5	5.72E-02	1.20E+02
E	1652	240.5	6.24E-02	1.10E+02
F	1652	293.1	7.61E-02	9.02E+01
G	1652-1406.4	N/A	5.90E-02	1.16E+02
H	1051	126.7	2.09E-02	1.64E+02
I	1051	129.8	2.14E-02	1.60E+02
J	1051	136.1	2.25E-02	1.53E+02
K	1051	145.9	2.41E-02	1.42E+02
L	1051	159.2	2.63E-02	1.31E+02
M	1051	176.5	2.91E-02	1.18E+02
N	1051	151.6	2.50E-02	1.37E+02

* See Figure 2.1-3 for Locations.

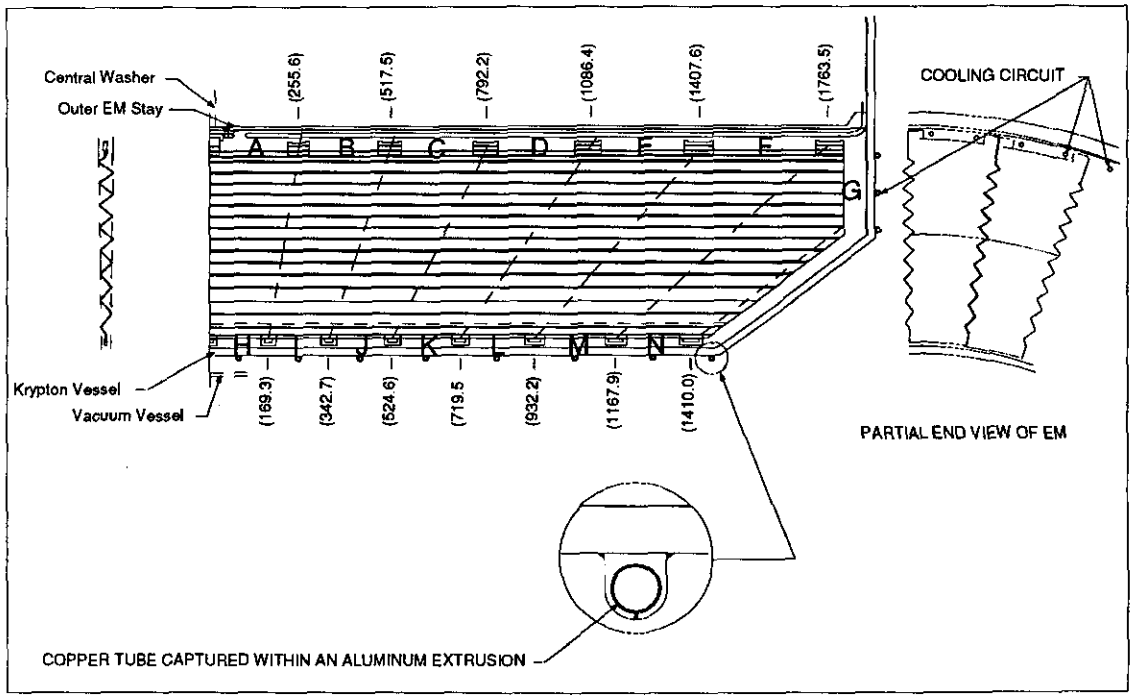

Figure 2.1-3 Barrel EM Module Cooling Loop & Circuit Board (A-N) Locations

There is also substantial heat leakage into the liquid vessel via radiation from the vacuum vessel jacket through the intervening multi layer insulation (MLI). Typical heat loss through a reasonably good blanket of MLI with an operational vacuum of 1.0e-6 torr is approximately 0.5 W/m^2. This results in losses of 9, 23, and 34 watts for the inner cylinder, both end heads, and the outer cylinder respectively. Table 2.1-3 summarizes the heat loads calculated for the various identified sources. It is conceivable that, at some time during the operational life of the detector, the insulating vacuum will become degraded or perhaps lost entirely, due to leakage, prolonged pump system failure, or deliberate shutdown for maintenance. Heat loads corresponding to these conditions are also listed in Table 2.1-3. The level assumed for the degraded insulation vacuum is 4.0e-4 torr. It is logical also to assume that electronics within the cryostat are automatically turned off in the event of complete vacuum loss. In the event of prolonged vacuum loss it is assumed that rapid transfer of LKr and LAr to emergency storage dewars will be initiated. The heat loads corresponding to total vacuum loss include both conduction and radiation effects. The conduction rate of 61 W/m^2 is based on gaseous nitrogen at atmospheric pressure and a 173 K temperature delta between the warm and cold walls.

Table 2.1-3 Barrel Calorimeter Heat Loads.

Component	**Heat Load (W)**		
Vacuum Level	**1.0 E-6 torr**	**4.0 E-4 torr**	**No Vacuum**
Preamplifiers			
Inner EM	1920	1920	n/a
Outer EM	3840	3840	n/a
Inner Hadronic	384	384	n/a
Outer Hadronic	144	144	n/a
Subtotals (W)	**6288**	**6288**	**n/a**
Vessel Shells			
Inner Cylinder	9	13	2016
Heads	23	33	5140
Outer Cylinder	34	48	7597
Subtotals (W)	**67**	**93**	**14753**
Feedthroughs	4400	4400	4400
Supports	190	190	190
Subtotals (W)	**4590**	**4590**	**4590**
Totals (W)	**10945**	**10971**	**19343**

2.2 End Cap Calorimeter Requirements

The EM and hadronic modules within each end cap calorimeter are distributed as shown in Figure 1-1. The circumferential distribution of these modules and the number of associated data channels is identified in Table 2.2-1. Typical end cap hadronic and EM modules with the location of motherboards and cables are illustrated in Figures 2.2-1 and 2.2-2, respectively. Table 2.2-2 summarizes the end cap heat loads for the various identified sources. As with the barrel the EM sections of the end cap calorimeters contain the highest concentration of electronics and require the highest level of cooling and control. The heat loads listed in Table 2.2-2 corresponding to total vacuum loss include both conduction and radiation effects. The conduction rate of 74.6 W/m^2 is based on gaseous nitrogen and a 213 K temperature delta.

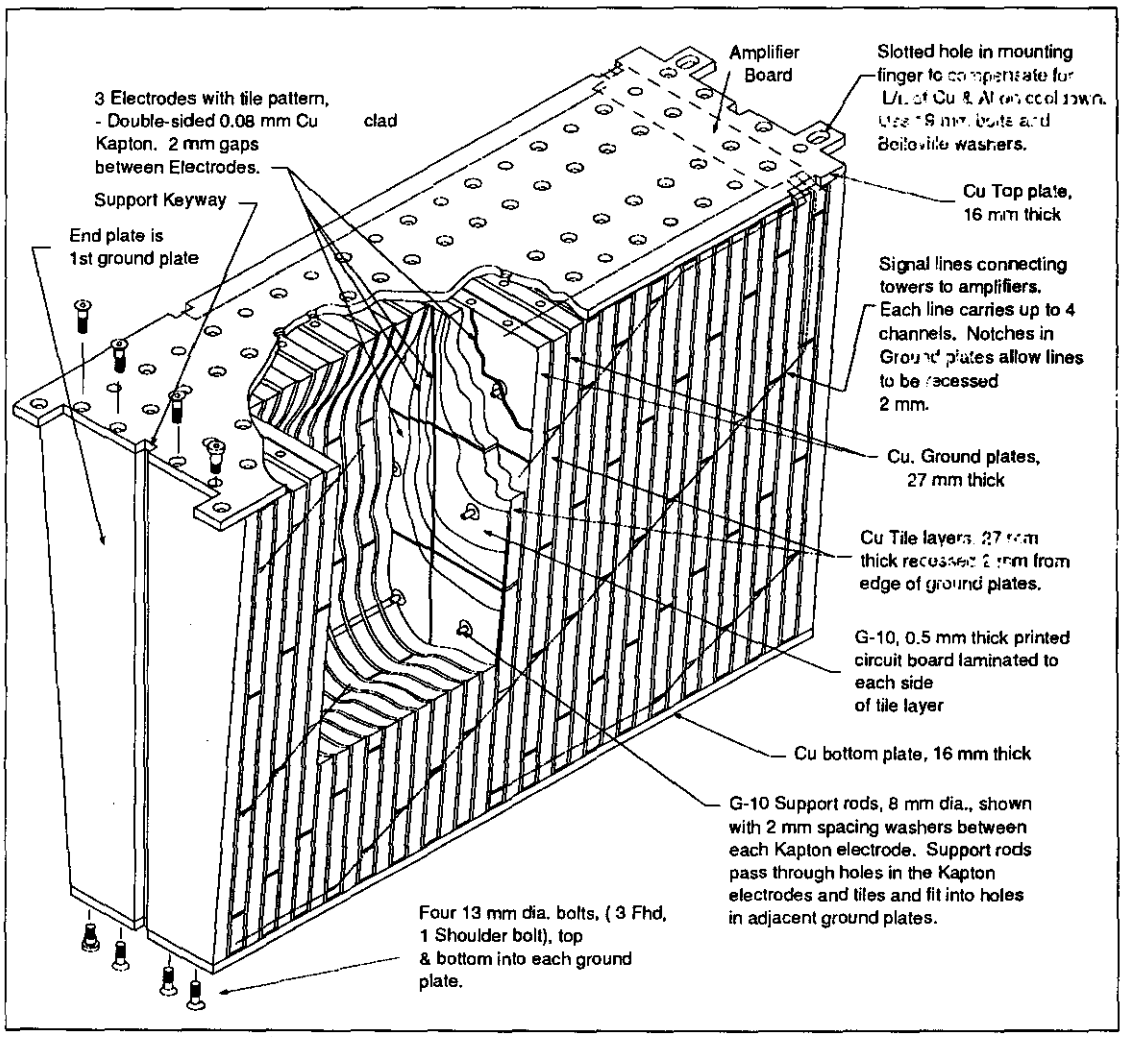

Figure 2.2-1 Typical End Cap Calorimeter Hadronic Module.

Table 2.2-1 End Cap Calorimeter Segmentation and Channel Count.

COMPONENT	SEGMENTATION $\eta \times \phi$ (x longitudinal)	*No. OF MODULES in ϕ	*No. OF CHANNELS
EM	.026 x .026, $1.23 < \eta < 1.83$	N/A	16,662
	.0522 x .0522, $1.83 < \eta < 2.46$	N/A	4,345
	.0783 x .0783, $2.46 < \eta < 2.95$	N/A	1,502
INNER HADRONIC A	.039 X .157, $1.31 < \eta < 1.73$	40	1723
	.078 X .157, $1.73 < \eta < 3.20$		3015
INNER HADRONIC B	.039 X .157, $1.48 < \eta < 1.89$	40	841
	.078 X .157, $1.89 < \eta < 3.39$		1538
INNER HADRONIC C	.039 X .157, $1.64 < \eta < 2.04$	40	821
	.078 X .157, $2.04 < \eta < 3.09$		1,077
OUTER HADRONIC A	.078 x .078	80	1,682
OUTER HADRONIC B	.078 x .078	80	2,462
OUTER HADRONIC C	.078 x .078	80	882

*Values Are Totals for Both Encaps.

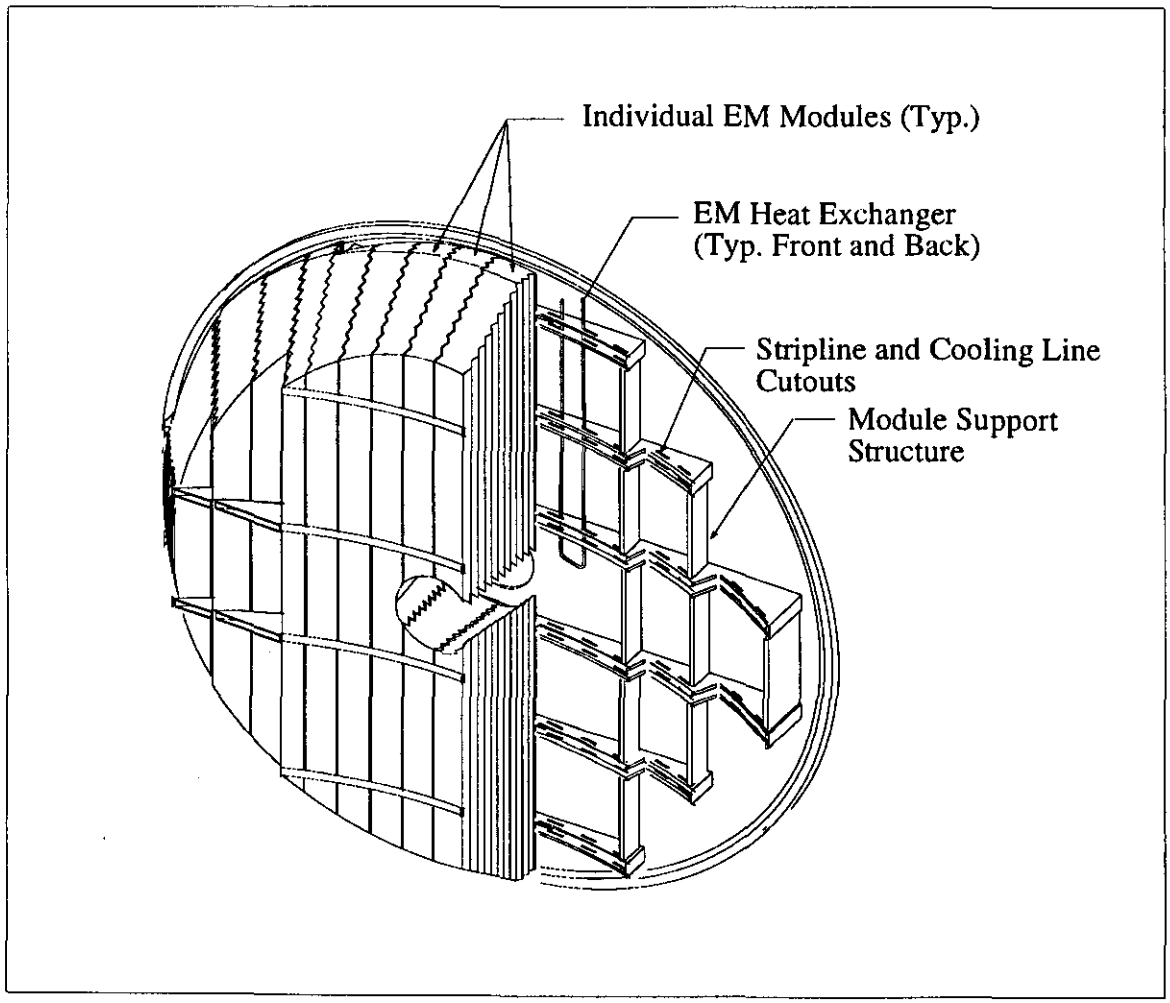

Figure 2.2-2 End Cap Calorimeter EM Section.

Table 2.2-2 Heat Loads for One End Cap Calorimeter.

Component	Heat Load (W)		
Vacuum Level	**1.0 E-6 torr**	**4.0 E-4 torr**	**No Vacuum**
Preamplifiers			
Forward EM	747	747	n/a
Aft EM	1493	1493	n/a
Inner Hadronic			
A	237	237	n/a
B	119	119	na/
C	95	95	n/a
Outer Hadronic			
A	84	84	n/a
B	123	123	na/
C	44	44	n/a
Subtotals (W)	**2942.0**	**2942.0**	**n/a**
Vessel Shells			
Inner Cylinder	1.4	2	377
Heads	25	34	6145
Outer Cylinder	27	37	6691
Subtotals (W)	**53**	**74**	**13212**
Feedthroughs	1900	1900	1900
Supports	160	160	160
Subtotals (W)	**2060**	**2060**	**2060**
Totals (W)	**5055**	**5076**	**15272**

3.0 THERMAL DESIGN CONCEPT

The current GEM calorimeter is based on liquid krypton and liquid argon as the ionization media in the barrel and the end caps respectively (Ref. 1). Table 3-1 lists some useful thermophysical properties of the two cryogens within the range of anticipated operating temperatures and pressures. As a result of the heat loads identified in the previous sections, active cooling is required to offset the thermal energy introduced into the ionization media by electronics, conduction and radiation through the vessel walls, supports, and feedthroughs. The concept, described in detail in the following sections,

Table 3-1 Thermophysical Properties of Liquid Argon and Liquid Krypton.

Property	Symbol	Liquid Argon (1)	Liquid Krypton (2)
Coefficient. Of Volume Expansion	β	7.1e-3 K^{-1}	3.31e-3 K^{-1} (3)
Density	ρ	1176 kg/m^3	~2420 kg/m^3
Specific Heat	Cp	1298 J/kg K	535 J/kg K
Viscosity	η	1.17e-4 Pa-s	4.31e-4 Pa-s
Thermal Conductivity	λ	8.66e-2 W/m K	9.05e-2 W/m K
Prandtl #	Pr	1.77	2.55 (3)

(1) Al Jaques, "Thermophysical Properties of Argon", TM-1517-A
(2) Encyclopedia of Chemical Technology, Table 4, Vol. 12, "Helium Group Gases".
(3) Derived Numerically.

uses a combination of internal and external heat exchangers to achieve the required thermal energy removal. Internal exchangers are used in areas of high thermal dissipation, such as near the electronics on the outer diameter of the barrel EM, where direct cooling of the ionization medium is required. The liquid vessel shells provide convenient mounting surfaces for external heat exchangers in areas of moderate thermal activity or where internal space is limited. The numerous penetrations for internal cooling loop crossovers provide adequate cooling for vessel heads in areas not associated with electronics.

3.1 Internal Cooling Circuits

To assure efficient thermal energy removal, the following guidelines were used in selecting the optimum routing of cooling lines and the placement of heat exchangers.

1. All cooling lines are placed near the heat sources,

2. Supply lines enter the cryostat at locations that are gravitationally above the corresponding return line penetrations to mitigate stratification within vessels,

3. Relatively short runs of inlet and outlet tubing were used between the heat exchanger and vacuum vessel wall to minimize heat gain in areas not associated with the intended target sources, and

4. The system is divided into separate, independent and symmetric sections to aid in uniform cooling and to provide redundancy.

3.1.1 Barrel Calorimeter Cooling Circuits.

Cooling Fluid - The baseline cooling system uses LAr as the heat exchanger fluid within the barrel calorimeter. This choice is based on the good thermophysical properties of LAr (Table 3-1) which allow it to be used at a reasonable operating pressure (~150 psi as compared to ~400 psi for LN_2) at LKr temperatures as well as the fact that contamination of the LKr by LAr due to cooling system leakage will not degrade calorimeter performance as severely as alternatives such as LN_2. It is also assumed that there will be a plentiful local supply of LAr since each end cap will use approximately 21,000 liters as the ionization medium. Table 3.1.1-1 lists flow rate requirements for the various barrel calorimeter parasitic heat sources. These rates were calculated assuming that 0.0197 l/minute of LAr is needed to remove one watt of heat energy. This cooling capacity is based on the enthalpy absorbed during a 2K rise in coolant temperature over a the range of pressure (142 - 182 psi) corresponding to the drop in pressure required to ensure even flow distribution within the heat exchanger loops. The value of specific heat for LAr is relatively insensitive to pressure changes in this range.

Design Concept - A schematic representation of the cooling circuit design which provides the total flow rates identified in Table 3.1.1-1 is shown in Figure 3.1.1-1. While providing the necessary cooling with two supply and eight return lines, this concept has not been optimized with respect to reliability considerations. In general high cooling system reliability will be achieved with few cryostat penetrations, in particular penetrations of the liquid vessel. However, failures in a system designed with few penetrations are likely to result in a large percentage loss of calorimeter coverage. Although the number of cryostat penetrations related to supply and return manifolding may change during the course of the optimization process, the overall internal design concept of the local heat exchangers will not be affected appreciably. The internal design features are described in the following paragraphs.

Table 3.1.1-1 LAr Coolant Flow Rates Associated With the Barrel Calorimeter Heat Loads Listed in Table 2.1-3.

Component	LAr Coolant Flow Rates (liters/minute)		
Vacuum Level	**1.0 E-6 torr**	**4.0 E-4 torr**	**No Vacuum**
Preamplifiers			
Inner EM	37.8	37.8	n/a
Outer EM	75.6	75.6	n/a
Inner Hadronic	7.6	7.6	n/a
Outer Hadronic	2.8	2.8	n/a
Subtotals	**123.9**	**123.9**	**n/a**
Vessel Shells			
Inner Cylinder	0.2	0.2	39.7
Heads	0.5	0.6	101.3
Outer Cylinder	0.7	0.9	149.7
Subtotals	**1.3**	**1.8**	**290.6**
Feedthroughs	86.7	86.7	86.7
Supports	3.7	3.7	3.7
Subtotals	**90.4**	**90.4**	**90.4**
Totals	**215.6**	**216.1**	**381.1**

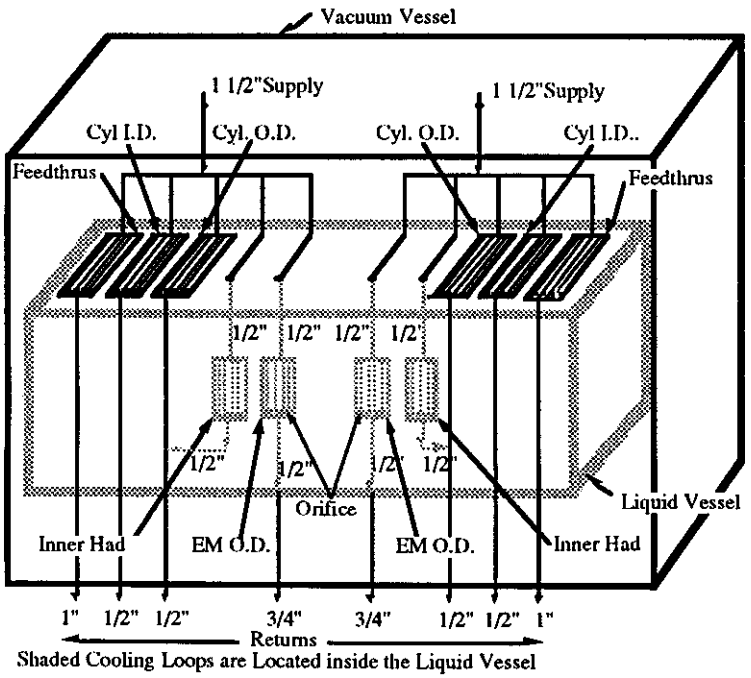

Figure 3.1.1-1 Barrel Calorimeter Cooling Line and Manifold Piping Sizes.

The proposed cooling system flow path for one end of the barrel calorimeter is illustrated in Figure 3.1.1-2. The EM section cooling circuit is divided into eight sections, each of which services one octant of the barrel. Figures 3.1.1-3 through 3.1.1-6 illustrate this arrangement which takes advantage of the calorimeter symmetry. Each octant is divided into two separate concentric circuits that service the inner and outer EM electronics.

Because of the limited space between the inner EM electronics and the liquid vessel cylinder the inner EM cooling loop is attached to the inside diameter of the aluminum vessel shell. The good thermal conductivity of aluminum at ~120 K provides a nearly uniform and stable cold wall near the electronics. The supply lines enter the cryostat vacuum space near the EM/Hadronic boundary and run radially into the ID of the inner vessel cylinder. There they turn and run axially into the barrel along the inner vessel wall to the barrel midsection. The return lines, located 90° around the circumference, follow

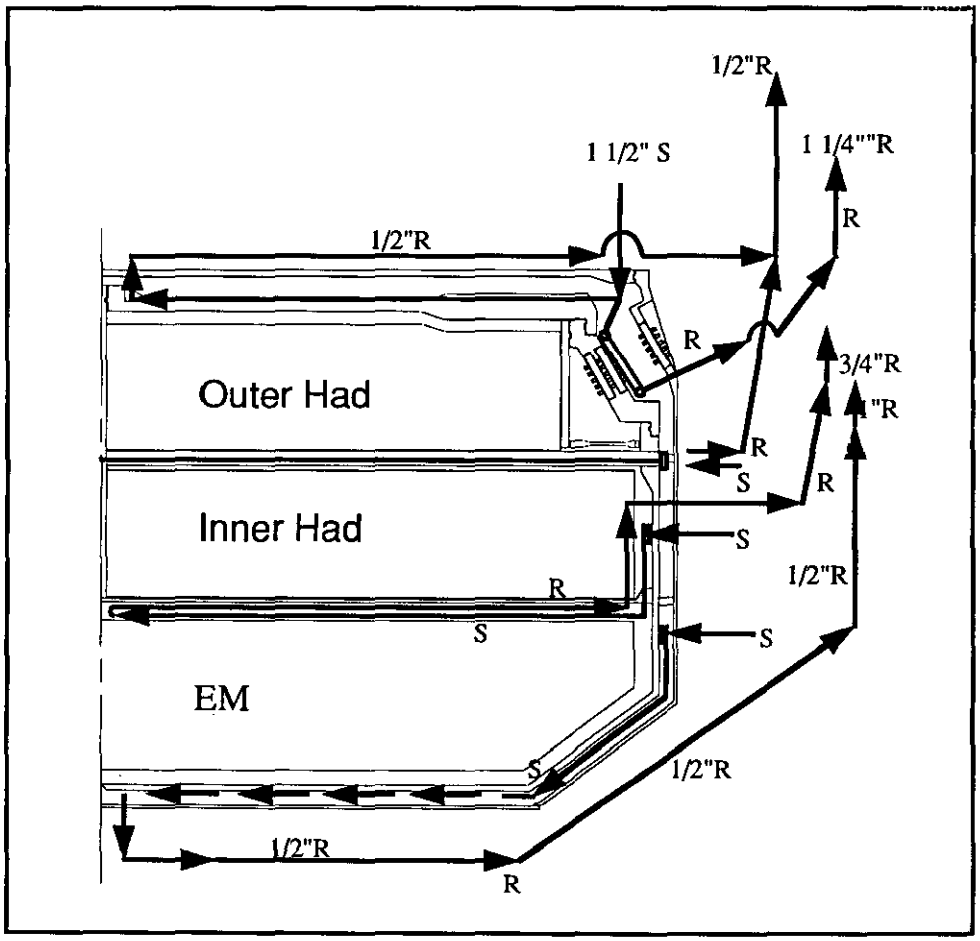

Figure 3.1.1-2 Flow Diagram For The Barrel Calorimeter Cooling Circuit.

the same routes but in the opposite directions. The supply and return are connected by heat exchange lines running as 90° arcs around the ID of the inner liquid vessel cylinder. There are 8 of these circumferential lines per octant each centered between two of the barrel EM inner tension strap raceways (Fig. 2.1-3). Three concentric circular heat exchanger circuits are mounted on the vessel head to provide cooling for the electronics mounted at the ends of the EM section (location G in Fig. 2.1-3). These lines are also divided into four 90 degree circumferential segments per barrel head. The proposed cooling line design uses a copper tube surrounded by an aluminum extrusion (Fig. 2.1-3 inset). This approach allows the heat exchanger assembly to be welded directly to the vessel wall assuring excellent heat transfer.

The electronics mounted on the outer diameter of the EM barrel are cooled by tubes located near the electronics in the space between the EM section OD and the surrounding outer aluminum shell. The "U" shaped loops are centered between adjoining modules. This positions them in the circumferential space between the module striplines that run axially along the top center of the EM modules. The arced end of the "U" is located at the module end nearest the calorimeter center. The supply and return ends of the loop turn outward and pass through the aluminum shell at the shell/head wall flange, immediately after which they penetrate the vessel end wall (Fig. 3.1.1-2).

It will probably be necessary to increase the "U" tube wetted surface area to achieve the required heat exchange between the copper tubing and the liquid krypton medium. Calculations and thermal modeling indicate that this can be accomplished by incorporating a perforated copper plate connecting the two legs of the loop along its length. This design also has the advantage of providing a more uniform average cooling temperature along a row of preamplifiers. Calculations performed to assess the performance of the barrel outer EM heat exchanger are documented in Appendix A.

Cooling requirements for the hadronic modules are much less stringent because of the greatly reduced heat load associated with the electronics. The inner hadronic section contains 20 heat exchanger loops placed within 57.15 mm diameter tubular aluminum structural stays that run the full length of the barrel (Fig. 3.1.1-4 and Ref. 4). One pair of these stays constitutes a single heat exchanger loop. The supply and return ends of a loop are located on the same end of the barrel, while the supply and return lines for adjacent

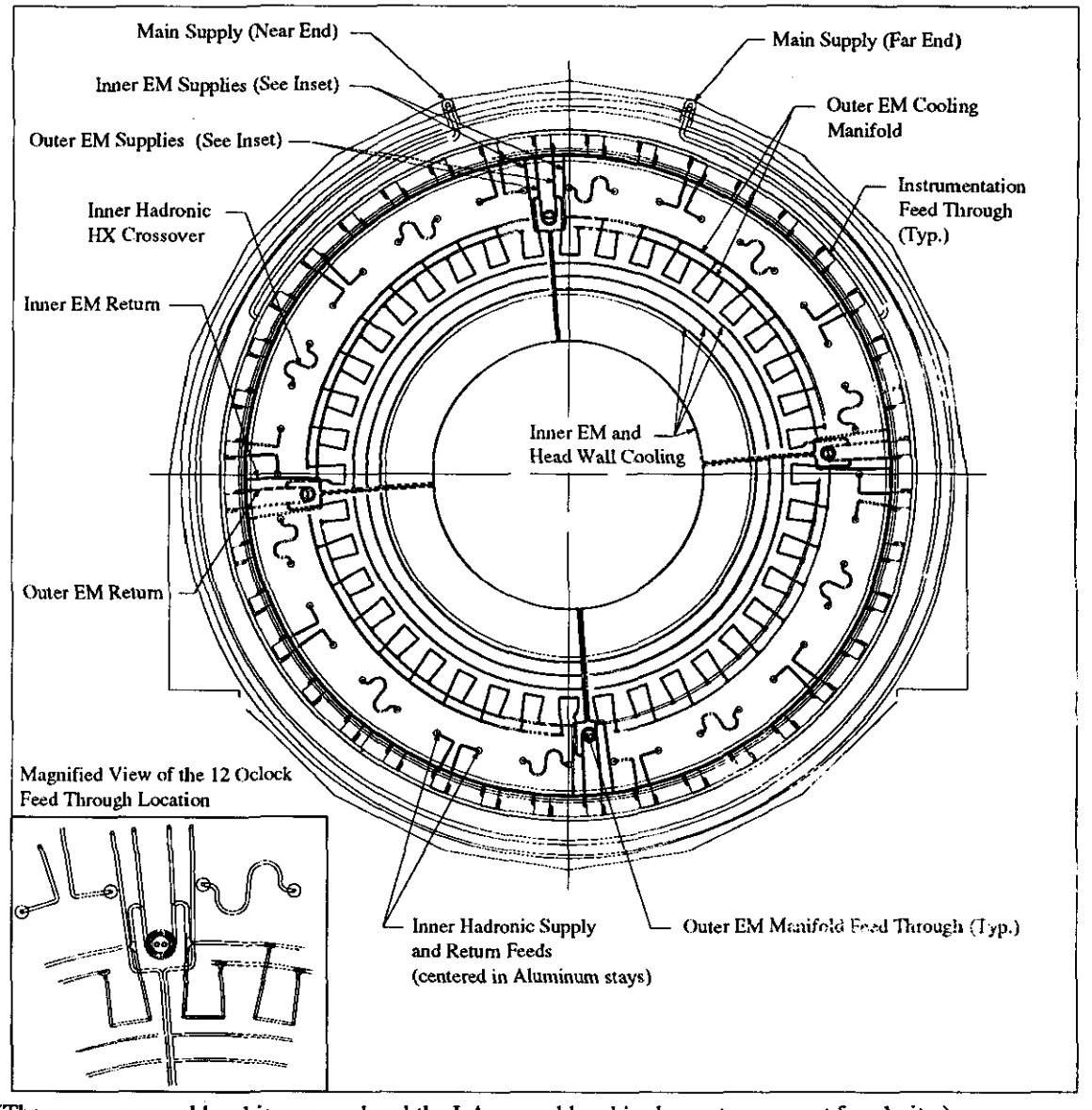

(The vacuum vessel head is removed and the LAr vessel head is shown transparent for clarity.)

Figure 3.1.1-3 Internal End View of Barrel Calorimeter Showing Cooling Circuit Pipe Routes.

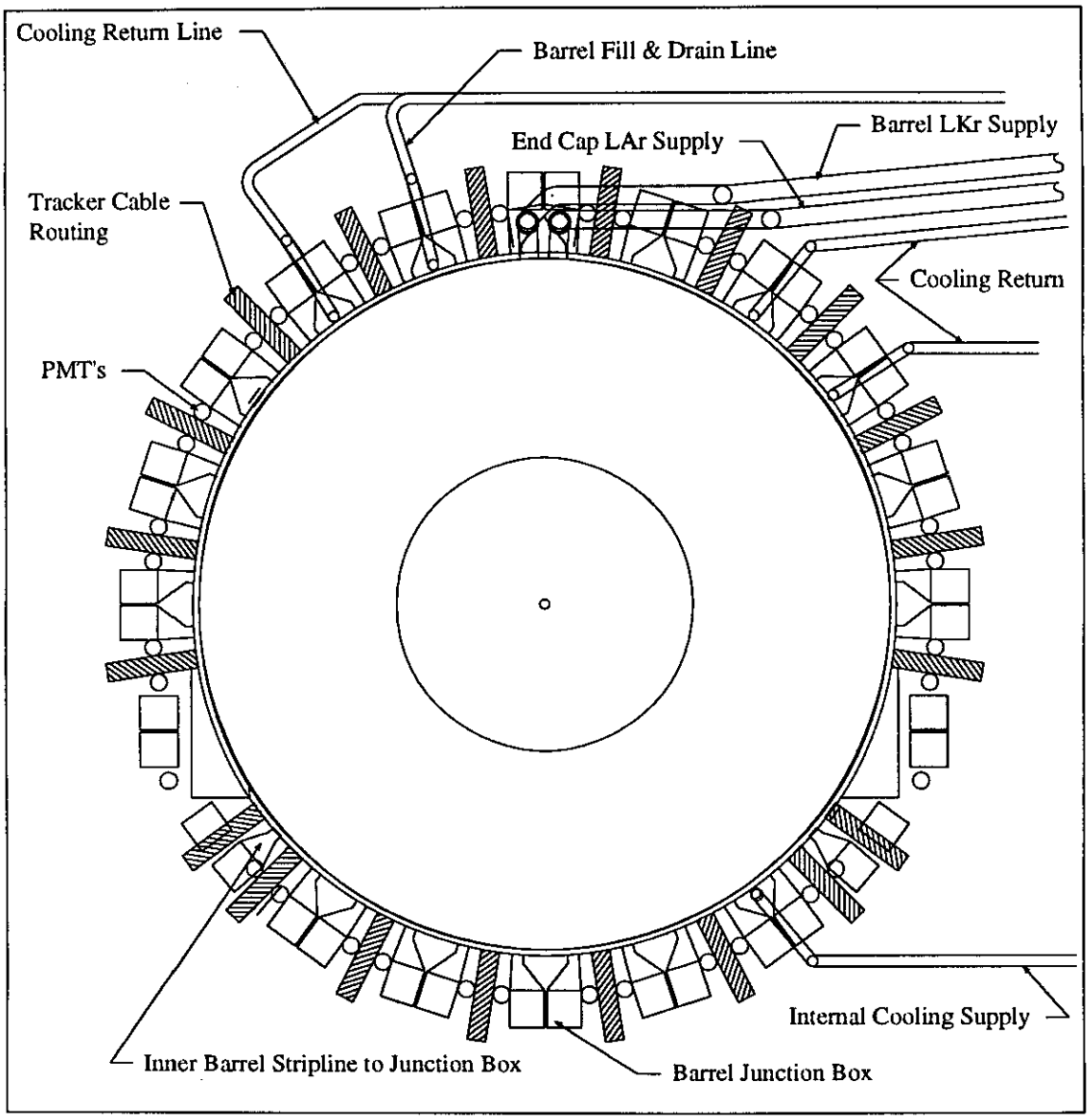

Figure 3.1.1-4 External End View of Barrel Calorimeter Showing the Routing of Utility and Instrumentation Lines.

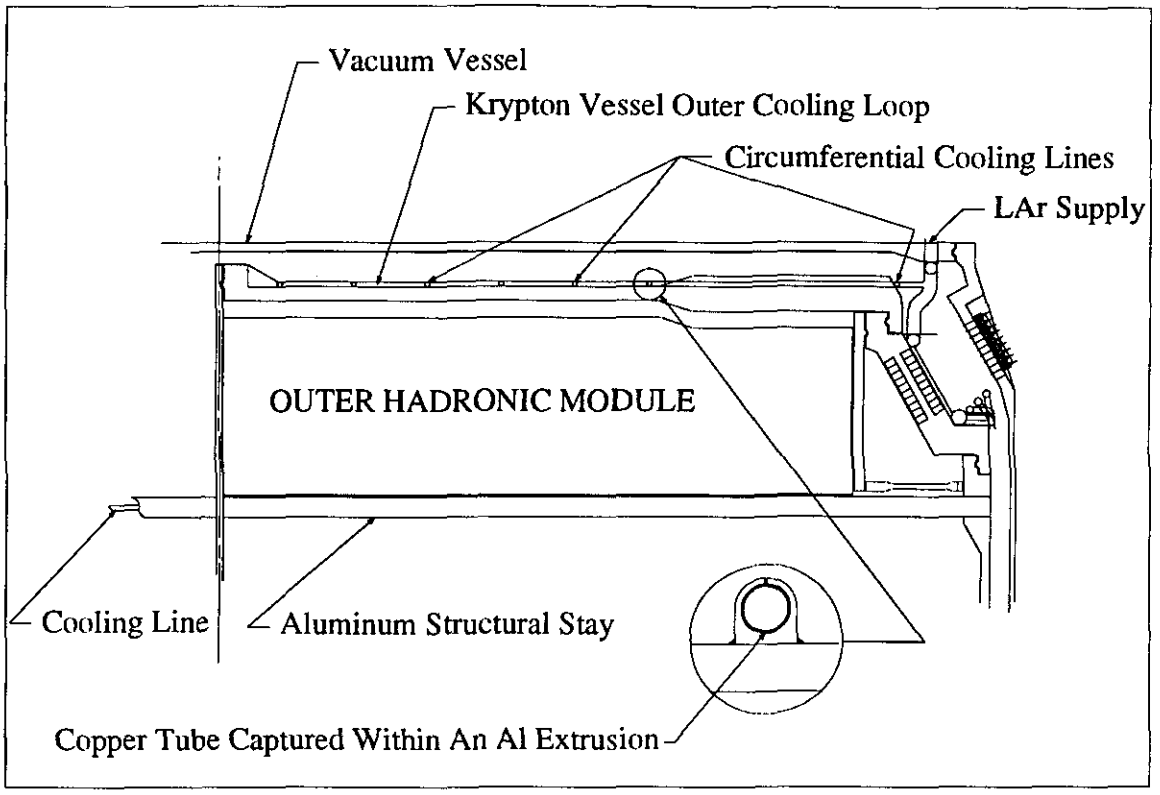

Figure 3.1.1-5 Barrel Hadronic and Outer Liquid Vessel Cooling Lines.

loops are located on opposite ends of the barrel in order to achieve more uniform cooling. "S" shaped crossovers designed to allow for differential thermal expansion and contraction complete the individual exchanger loops at the ends of the barrel opposite the supply and return feeds (Fig. 3.1.1-3).

The outer hadronic modules are cooled in a manner similar to the inner EM electronics. Figure 3.1.1-5 shows one of eight heat exchanger loops (one for each octant of the barrel) located along the outside of the outer liquid vessel wall that will actively cool the outer shell and effectively intercept any thermal energy transmitted across the vacuum space. The legs of each loop are cross connected by equally spaced lines that run 90 degrees around the circumference. The aluminum liquid vessel shell will in turn act as a uniform cold wall to remove heat generated by the outer hadronic module electronics. The axial lines for each of these loops lie in grooves machined into the thick end sections of the vessel so that they will not interfere with the vessel support strap. Conduction in this

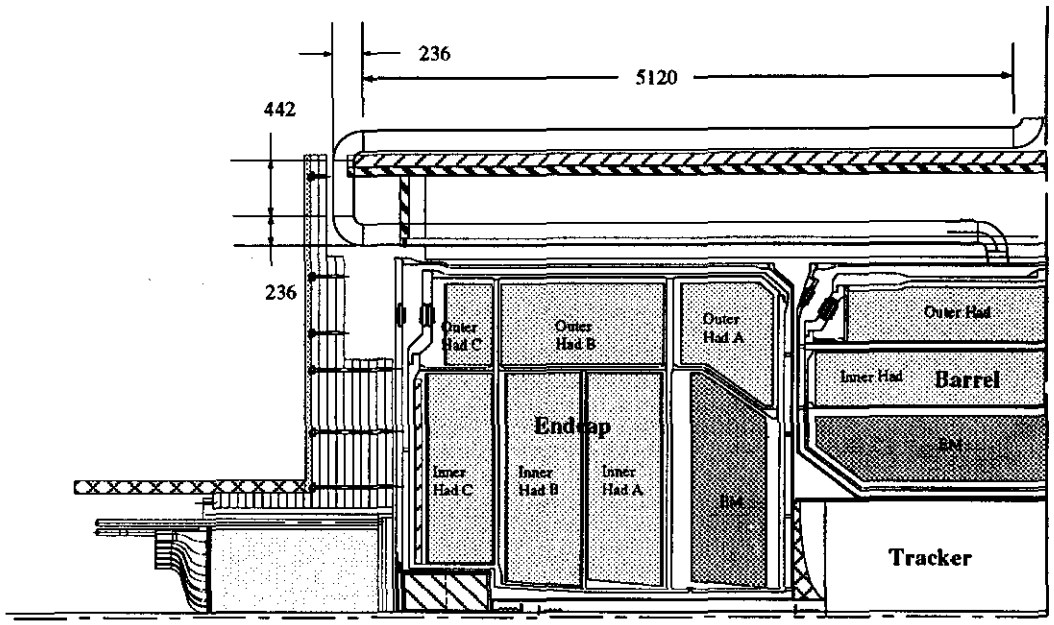

Vacuum Lines

Vacuum Port: 5120
442
4808
10370 mm ±

4-5 90° Long Radius Elbows

LKr Supply Vacuum Jacket Line

5120
300
4808
10228 mm ±

4-5 90° Long Radius Elbows
1 - 8" x 6" Reducer

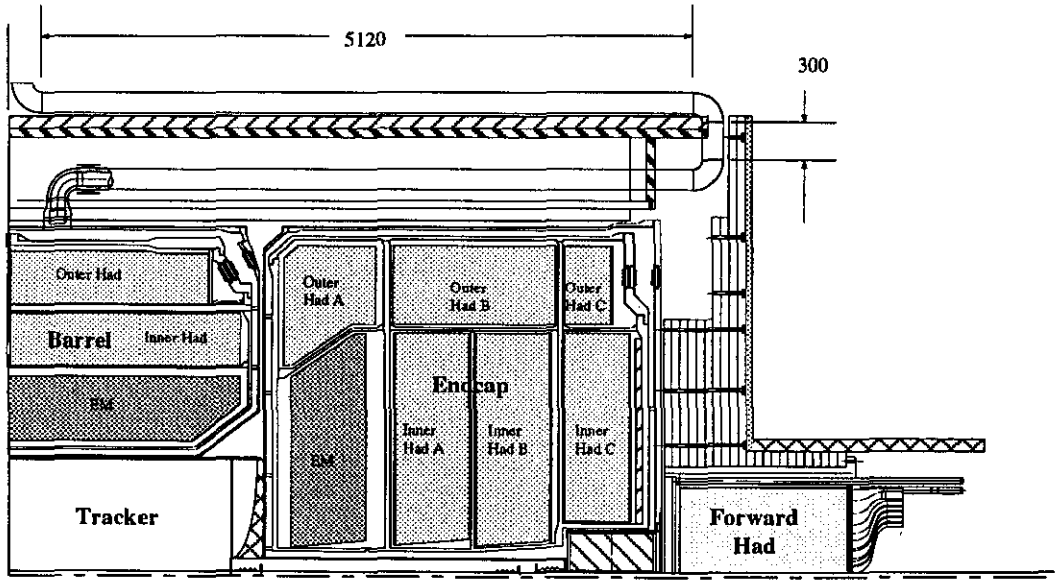

Figure 3.1.1-6 Barrel Calorimeter Vacuum and LKr Supply Line Routes.

relatively thick aluminum region is adequate enough to preclude the need for circumferential cross connecting lines in this area. The pipe design is identical to that proposed for the inner EM cooling circuit with a copper tube trapped within an aluminum extrusion (Fig. 3.1.1-5 inset). This design allows the assembly to be welded directly to the vessel and provides excellent heat transfer.

There are several tradeoff issues regarding the choice of heat exchanger (HX) line geometry in any section. For example, in the case of the inner hadronic Section we have baselined 0.5 inch bore holes in the aluminum structures which will in turn house 0.5 inch OD copper tubing. These tubes must carry rod inserts/spacers to provide good heat transfer and pressure drops that will ensure even flow distribution in the 20 parallel lines. For the required mass flow rate and temperature rise along the line, a certain value of the hydraulic diameter ($D_H = D_{1out} - D_{1in}$) is needed. Therefore the gap established by the rod insert is critical because the pressure drop is very sensitive to D_H . If the wall thickness is too small the tube will crack when expanded against the aluminum, but if it is too large the gap size tolerance will be difficult to achieve. Table 3.1.1-2 illustrates one possible set of heat exchanger dimensions to achieve the required performance.

Table 3.1.1-2 Summary of Barrel Calorimeter Heat Exchanger Design Results.

Heat Exchanger Description	No. of HX Circuits	Heat Load/ Circuit (W)	LAr Flow Rate (kg/s)	Hydraulic Diameter (mm)	Line Length (m)	N_R	ΔP/ Circuit (psi)
Inner EM 3/16" OD x .045" Wall Cu 8 per octant, 90° Circumferential External indirect cooling	64	30	1.3e-2	2.47	1.7	5.7e4	6.4
Outer EM (See Appendix A) 3/16" OD x .030" Wall Cu "U" Tubes with plate 10 per octant, internal direct cooling	80	48	2.0e-2	3.24	4.0	6.7e4	8.8
Inner Hadronic 1/2" OD x .065" Wall Cu "U" Tubes with 11/32" rod inserts 20 - Full Length of barrel internal direct cooling	20	19.2	8.0e-3	0.67	8.0	1.3e5	8.3
Outer Hadronic 1/8" x .030" wall Cu 90° Circumferential, 7 per Octant external indirect cooling	56	3.2	1.3e-3	1.65	4.3	8.6e3	2.0
Note: OD & Wall thickness may be increased to increase surface contact areas.							

3.1.2 End Cap Calorimeter Cooling Circuits

Although the basic cooling circuit design for the endcap incorporates many of the same concepts as used in the barrel calorimeter the end cap system differs from the barrel in several important ways. For example, the end cap system will employ LN_2 to cool the LAr ionization medium, and the end cap system supply and return lines must also be designed to facilitate movement of an end cap to allow for maintenance access to the barrel calorimeter and tracker.

The design concept of the end cap cooling circuits is less mature than that for the barrel, however, Figures 3.1.2-1 through 3.1.2-3 illustrate preliminary candidate locations. Figure 2.2-2 also shows the proposed heat exchanger location for the EM. Each end cap quadrant is serviced by four systems consisting of four circuits each, except for the inner cylinder system, which, because of its small diameter (~394 mm) will probably require only a single circuit per end cap. The EM circuits can be mounted to the EM support structure near the fore and aft surfaces where the electronics are to be mounted. The hadronic electronics cooling circuits rely primarily on cooling of near by vessel shells and washers.

Table 3.1.2-1 lists flow rate requirements for the various end cap calorimeter parasitic heat sources. These rates were calculated assuming that 0.0177 l/minute of LN_2 is needed to remove one watt of heat energy. This cooling capacity is based on the enthalpy absorbed during a 2K rise in coolant temperature beginning at approximately 84.5 K.

As was the case for the barrel, the EM section electronics produce the highest concentration of heat within the end cap. There are approximately 11,250 EM preamplifiers per end cap, with 3750 and 7,500 mounted on circuit boards at the forward and aft faces of the EM section respectively.

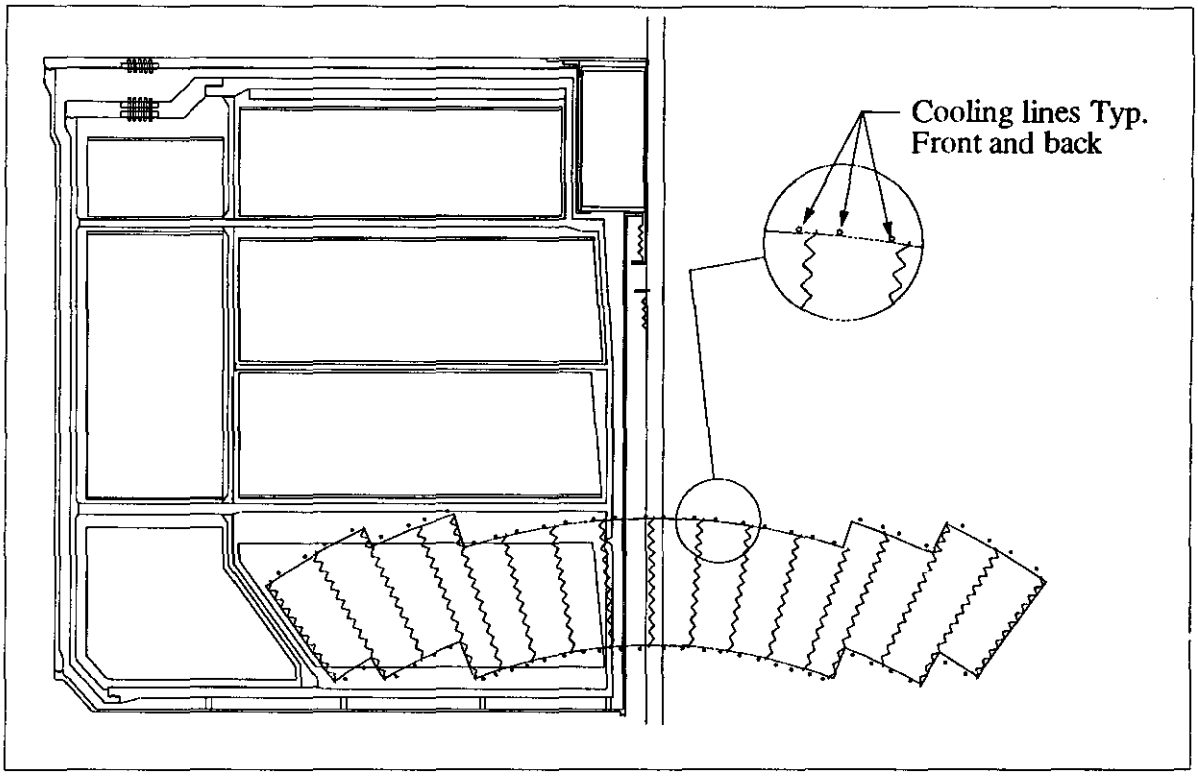

Figure 3.1.2-1 Top View of End Cap Calorimeter Showing Proposed EM Heat Exchanger Locations.

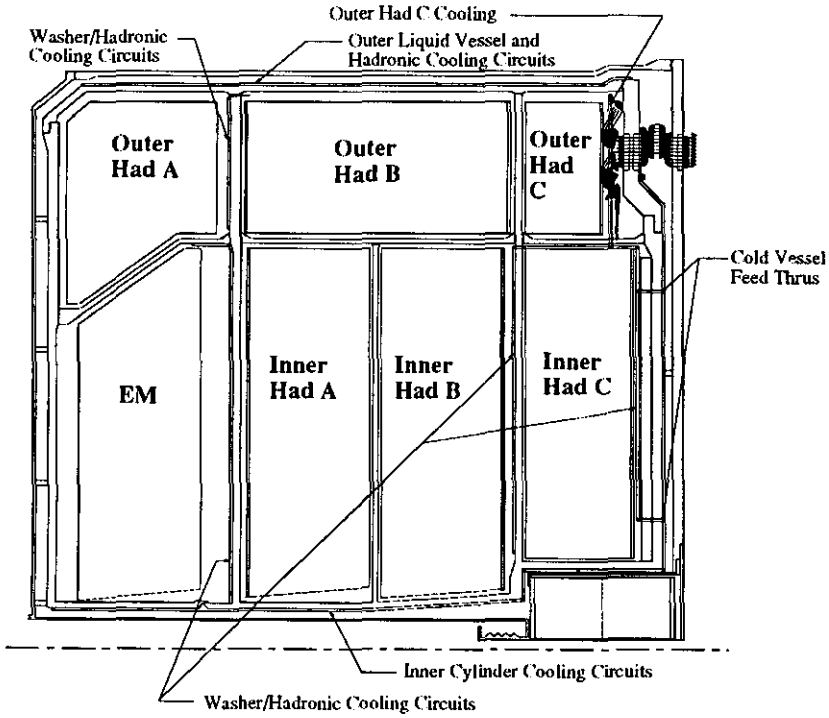

Figure 3.1.2-2 Preliminary Cooling Circuit Routes for the End Cap Calorimeter.

Table 3.1.2-1 LN_2 Flow Rates Associated With The End Cap Heat Loads Listed In Table 2.2-1 (Values Are for One End Cap Only).

Component	LN_2 Coolant Flow Rates (liters/minute)		
Vacuum Level	**1.0 E-6 torr**	**4.0 E-4 torr**	**No Vacuum**
Preamplifiers			
Forward EM	13.2	13.2	n/a
Aft EM	26.4	26.4	n/a
Inner Hadronic			
A	4.2	4.2	n/a
B	2.1	2.1	na/
C	1.7	1.7	n/a
Outer Hadronic			
A	1.5	1.5	n/a
B	2.2	2.2	na/
C	0.8	0.8	n/a
Subtotals (W)	**52.1**	**52.1**	**n/a**
Vessel Shells			
Inner Cylinder	0.0	0.0	6.7
Heads	0.4	0.6	108.8
Outer Cylinder	0.5	0.7	118.4
Subtotals (W)	**0.9**	**1.3**	**233.9**
Feedthroughs	33.6	33.6	33.6
Supports	2.8	2.8	2.8
Subtotals (W)	**36.5**	**36.5**	**36.5**
Totals (W)	**89.5**	**89.8**	**270.3**

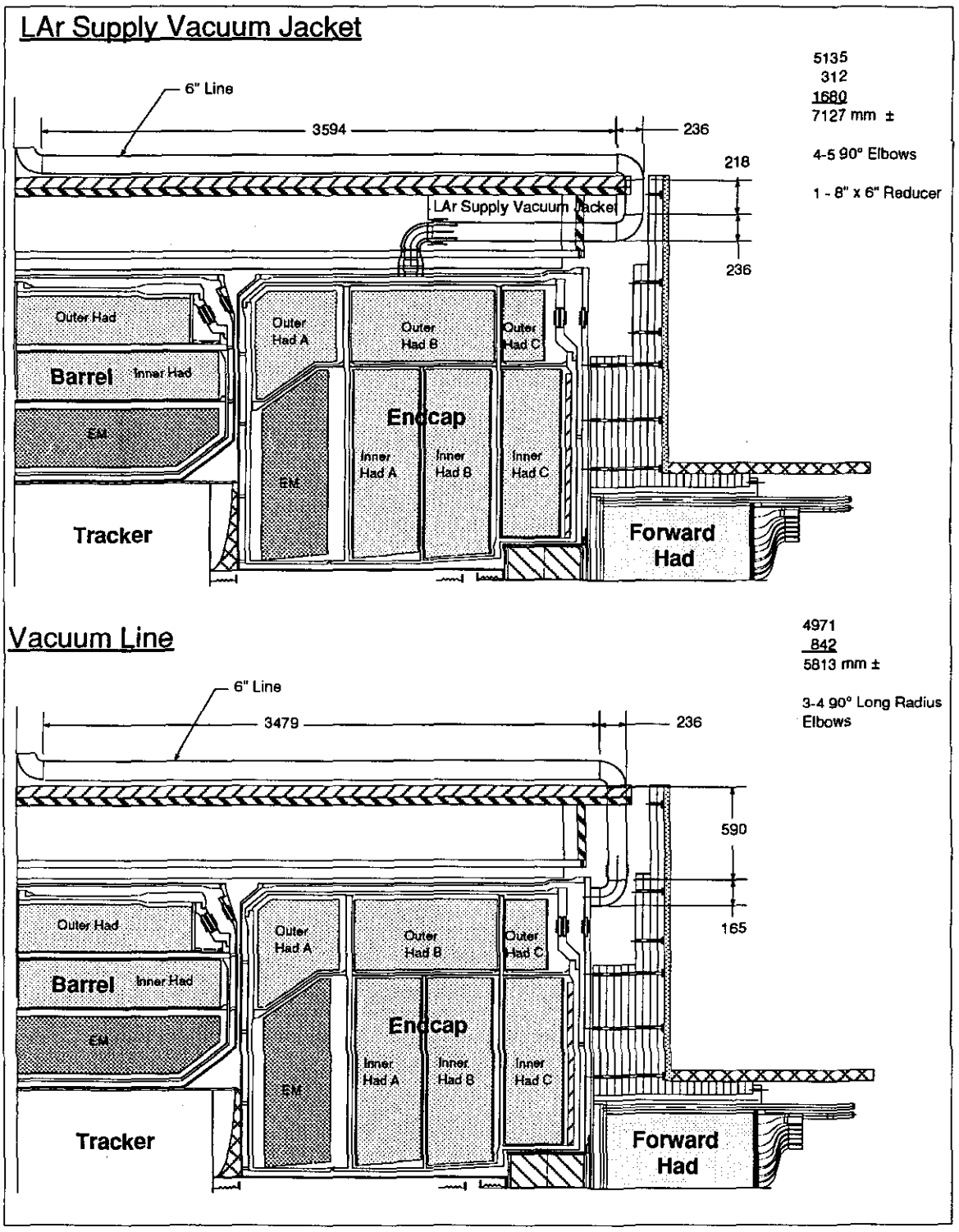

Figure 3.1.2-3 End Cap Calorimeter Vacuum and LAr Supply Routes.

3.2 Feedthroughs

The largest collective number of penetrations of the cryostat are those required to pass the calorimeter signal cables to the outside environment. The GEM baseline design calls for 160 of these signal cable feedthroughs. to service approximately 128,000 channels of data plus another 14,000 power, calibration, control, and monitoring circuits. Design details of these high density cryogenic feedthroughs are provided in Reference 5. Preliminary, conservative analyses indicate that these feedthroughs constitute the largest heat leak to the calorimeter. Cooling line, vacuum line and fill/drain line feedthroughs also constitute potential heat leaks to the calorimeter interior.

Barrel Calorimeter Feedthroughs - Each of the 80 (40 on each end) signal feedthroughs is assumed to service approximately 900 data channels. This number includes an approximate 10% overhead to cover calibration, high voltage supply, and monitoring circuits. The signal wire is stripline cable in which each signal line comprises 3 copper traces, one signal and two shields, separated by 0.13 mm thick KAPTON dielectric. Each signal trace is 0.254 mm wide by 0.3272 mm thick and each shield trace is 63.5 mm wide by .0164 mm thick. This results in a copper conductor cross section of 0.166 mm^2 for each of the 25 signal line sets in a strip line. The cable length between the cold and the warm vessel wall feedthroughs is approximately 200 mm. Reference 6 lists the integrated thermal conductivity for high purity copper as 73 W/mm from 120 K to 300 K. The corresponding heat leak for 72,000 signal/shield sets is about 4.4 kW.

Figure 3..2-1 shows that cooling is provided by concentric heat exchanger tubes running along the inner and outer radii of the ring of feedthroughs. The system is also divided into octants with four 90 degree circumferential circuits per barrel end.

Bellows feedthroughs are used for the main LKr supply lines where they penetrate the cryostat. Bellows allow for the relative motion of lines and vessel shells resulting from differential thermal expansion and contraction effects. Bellows also serve to thermally and acoustically isolate sections of the system and as such are used to both increase the thermal length between warm and cold surfaces and to mitigate transmission to the calorimeter of vibrations from down stream mechanical blowers and pumps.

Because the supply lines and bellows are stainless steel, and the vessel walls are

aluminum, the feedthroughs must also be able to accommodate transitions across dissimilar metals while remaining leak tight. This is accomplished by incorporating bi metallic joints which allow the feedthroughs to be seal welded to both the aluminum vessel walls and the stainless steel lines. Concepts for the main LKr supply and vacuum feedthrough ports are illustrated in Figure 3.2-3.

The close proximity of penetrations for adjacent outer EM manifold octants suggests that one feedthrough can service two lines. The configuration of a such a feedthrough depends on its location, for example, the feedthrough at the 12 o'clock position of the outer EM cooling circuit manifold services two supply lines, the 3 and 9 o'clock positions each service a pair of supply and return lines, and the feedthrough located at the 6 o'clock position services two return lines (Fig. 3.1.1-3). These feedthroughs also incorporate bi metallic joints to allow the feedthroughs to be seal welded to both the stainless steel cooling system lines and the aluminum vessel.

All vacuum vessel penetrations incorporate bellows feedthroughs mounted external to the vessel insuring that they remain externally pressurized in order to mitigate bellows squirm (Figure 3.2-3).

The inner hadronic cooling loops do not require bellows feedthroughs at the liquid vessel head penetrations because they are routed through the aluminum stays which are seal welded to the vessel heads. The outer hadronic and inner EM loops do not penetrate the liquid vessel.

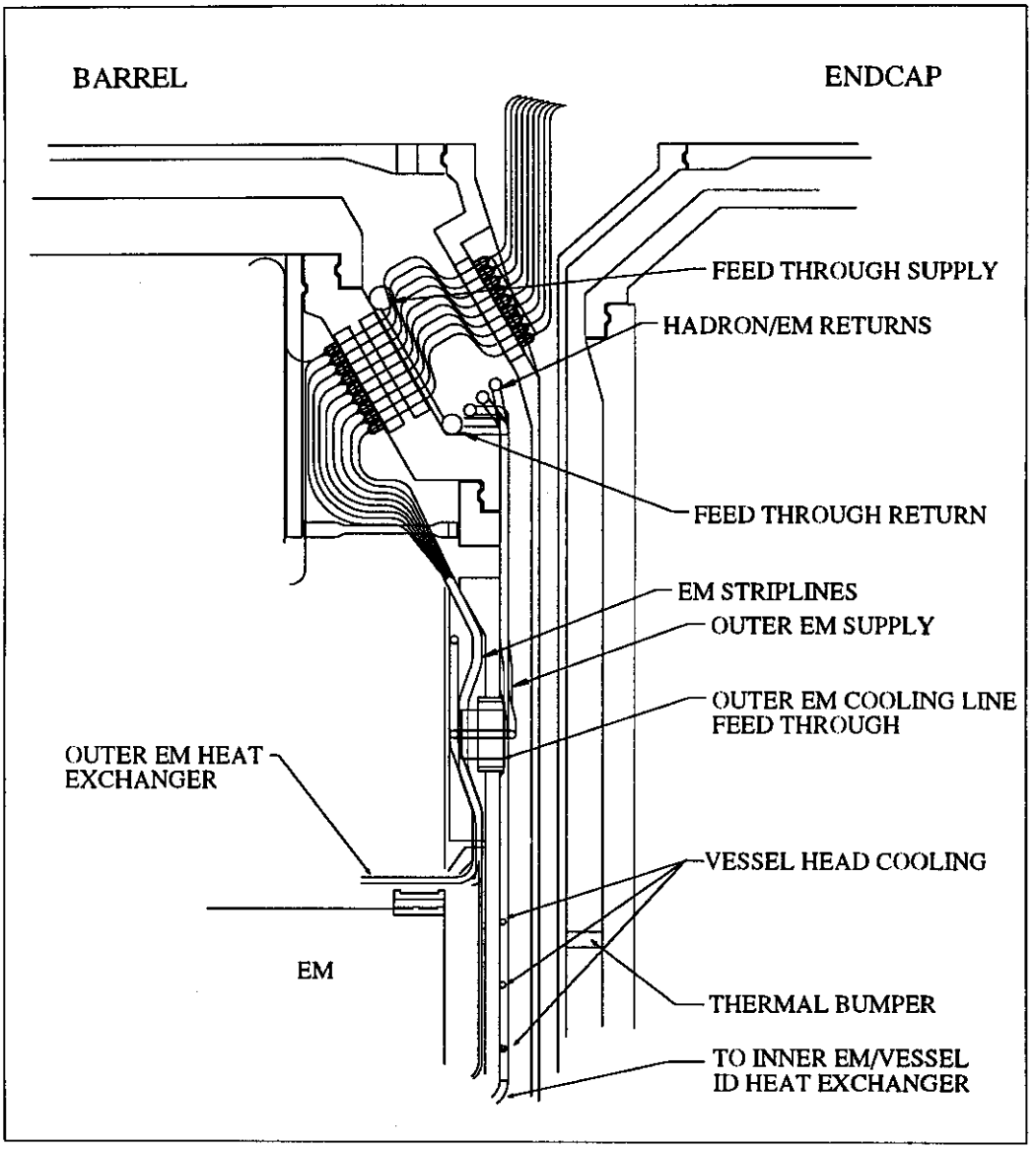

Figure 3.2-1 View of Barrel Calorimeter Signal Cable Feedthrough Showing the Associated Cooling Circuit Layouts.

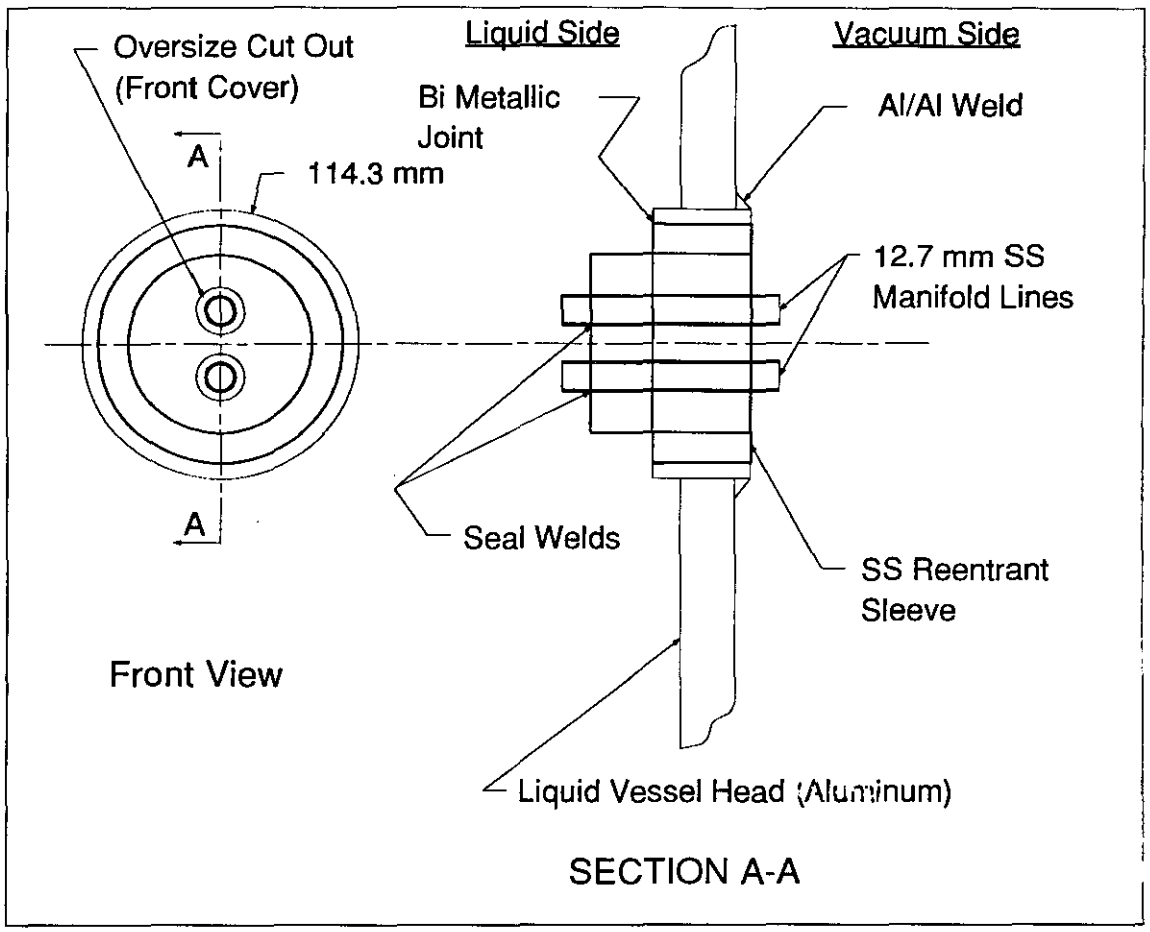

Figure 3.2-2 Barrel Calorimeter Outer EM Supply and Return Manifold Cold Feedthrough Concept.

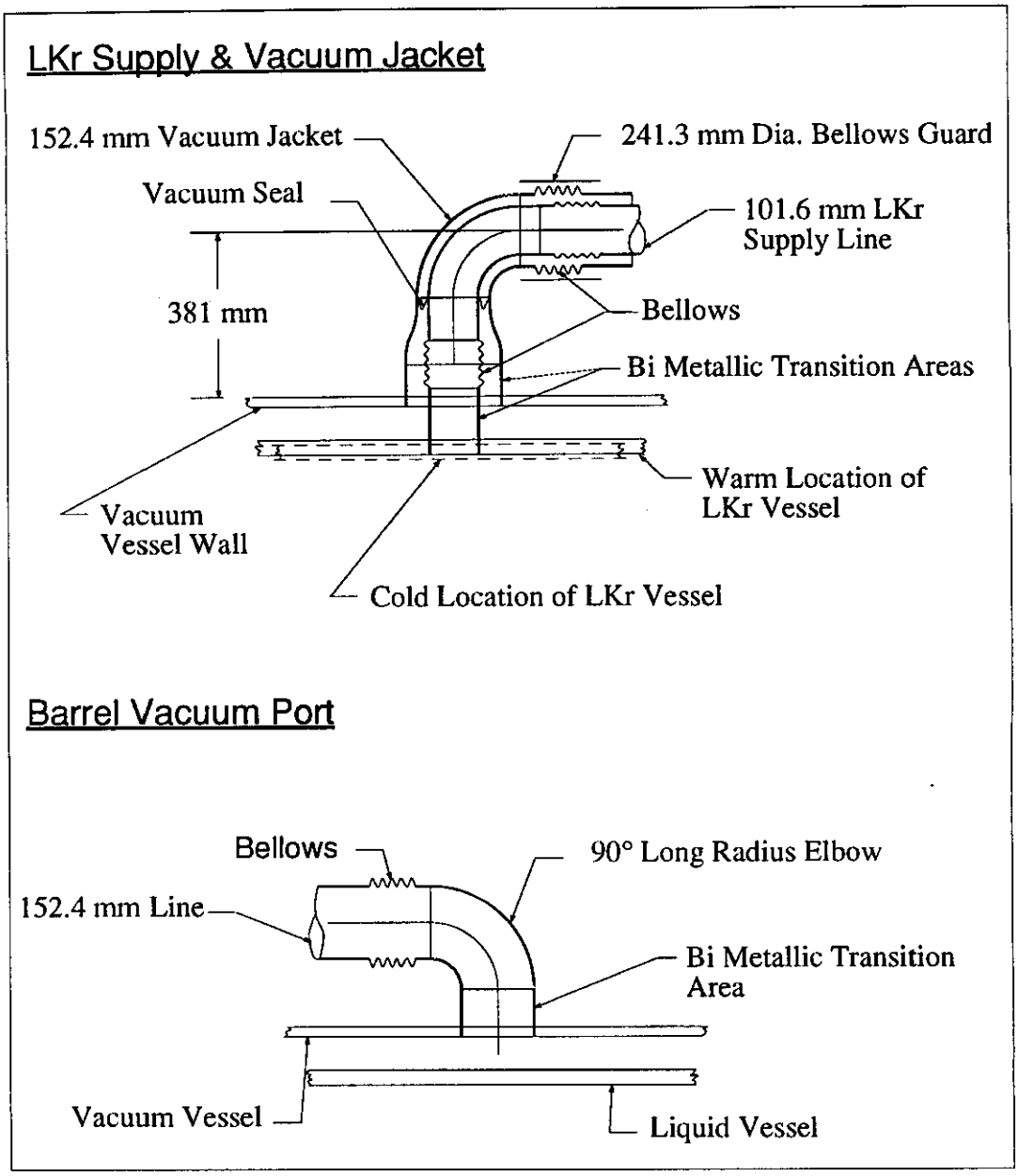

Figure 3.2-3 Barrel Calorimeter LKr Supply Line and Vacuum Port Details.

End Cap Calorimeter Feedthroughs - The GEM baseline design incorporates 40 data signal feedthroughs for each end cap. The feedthrough design is essentially the same as that for the barrel with each servicing approximately 875 signal, high voltage power, calibration, and monitoring/control circuits (Fig. 3.2-4). The stripline cables connecting the cold and warm halves of an end cap feedthrough are all approximately 275 mm in length. Reference 6 lists the integrated thermal conductivity for high purity copper as 91

W/mm from 80 K to 300 K. The corresponding heat leak for the ~35,000 signal/shield sets of one end cap is, therefore, about 1.9 kW.

Figure 3.2-4 shows that cooling of the end cap feedthroughs is similar to that proposed for the barrel which is provided by concentric heat exchanger tubes running along the inner and outer radii of the ring of feedthroughs. The system is also divided into octants with four 90 degree circumferential circuits per end cap. Details of the end cap signal feedthrough design are also provided in Reference 5.

Cooling circuit and vacuum system bellows feedthroughs for the end cap are identical in concept to those discussed previously for the barrel calorimeter. The proposed LAr supply line feedthrough and vacuum ports are shown in Figure 3.2-5.

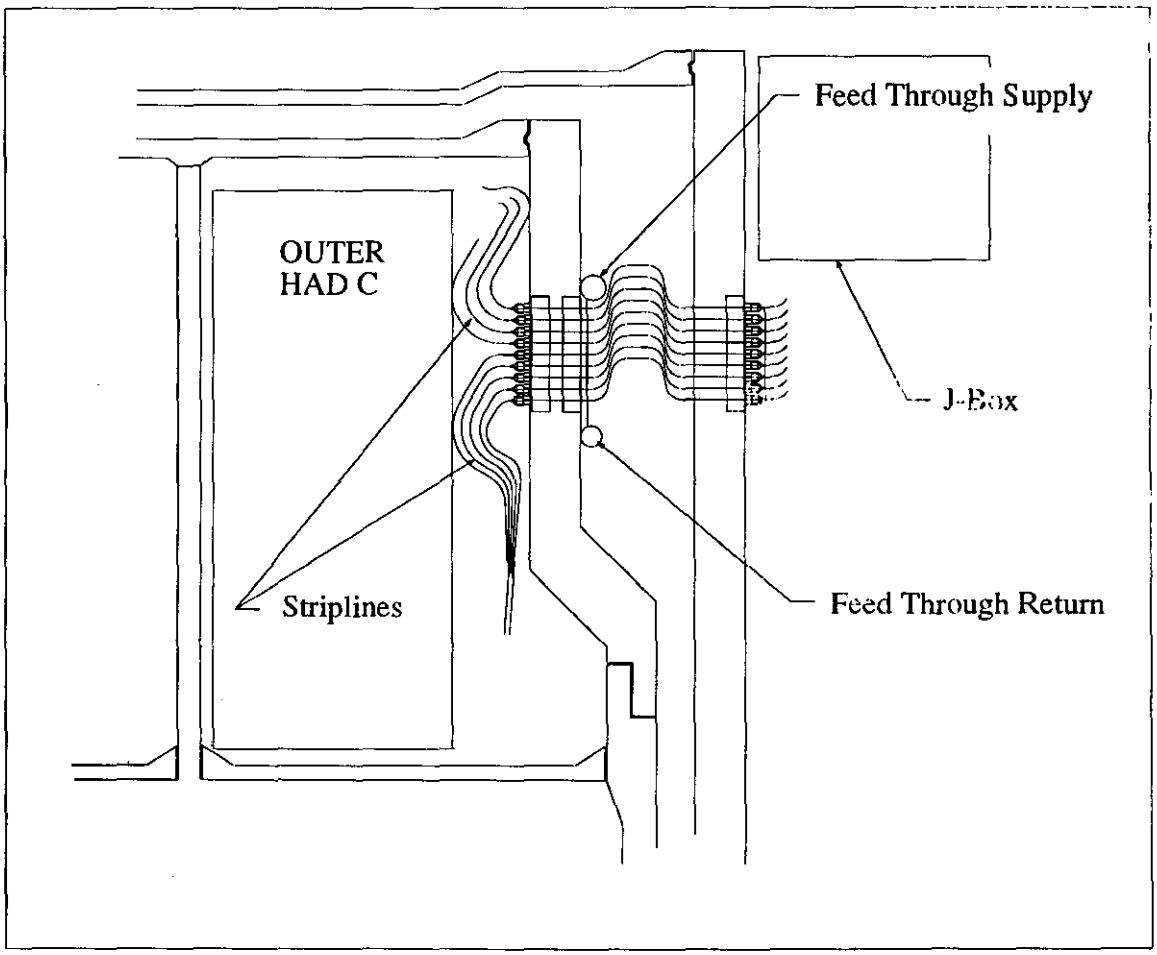

Figure 3.2-4 End Cap Signal Cable Feedthrough and Associated Cooling Lines.

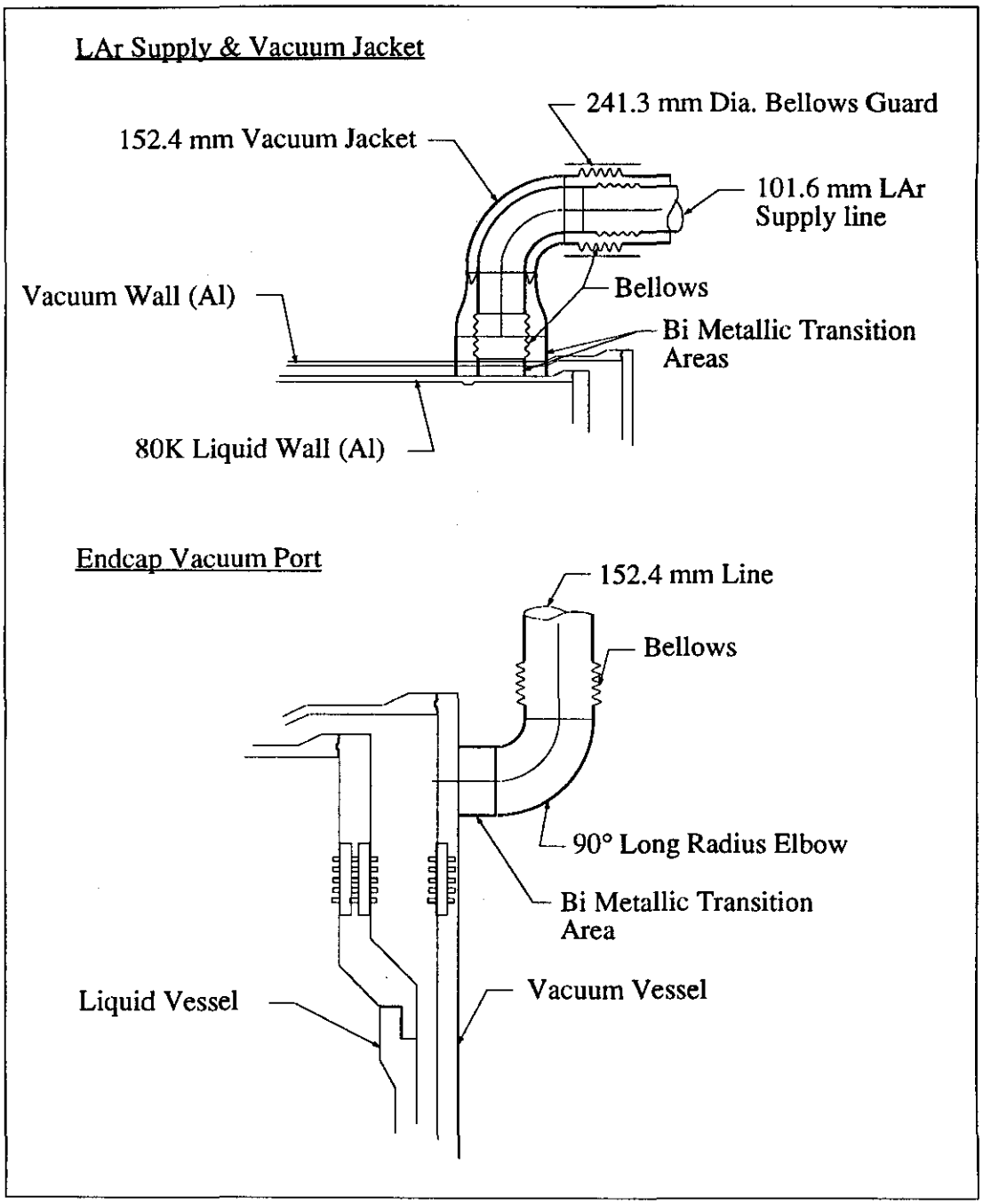

Figure 3.2-5 End Cap LAr Supply Line and Vacuum Port Details.

3.3 Support Stanchions

The barrel and end cap support stanchions are very similar in design to those developed for the DØ detector. Figure 3.3-1 shows a typical stanchion which incorporates a thermal

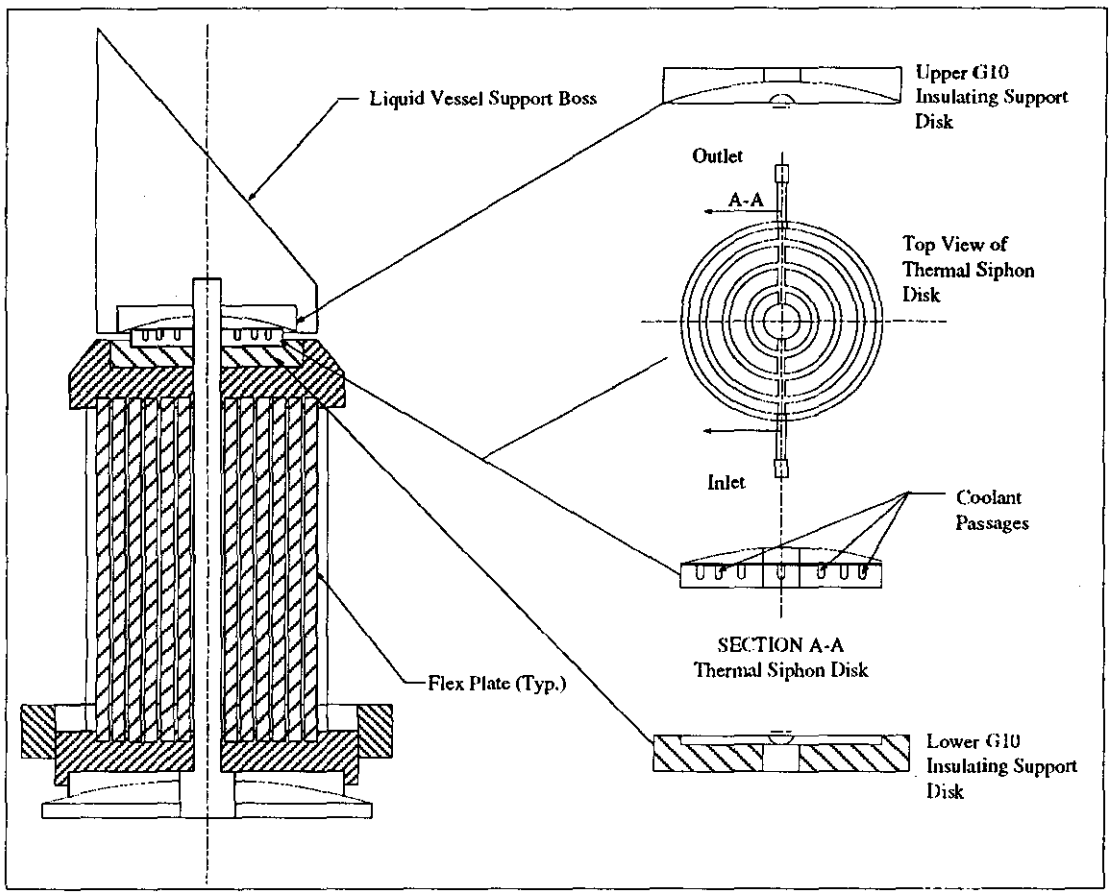

Figure 3.3-1 Typical GEM Calorimeter Support Stanchion With Thermal Intercept Details

intercept constructed of a flat circular stainless steel disk with machined grooves through which liquid argon coolant is circulated via a thermosiphon circuit. A machined concave top plate forms the gas tight cover. The assembled intercept plate fits between thermally insulative upper and lower G-10 support disks. This design results in a modest total heat load of approximately 191 Watts total for the four barrel supports and 160 W for each 389 Mg end cap. The corresponding LAr (barrel) and LN_2 (end cap) coolant flow rates, assuming 2K deltas, are 3.7 and 2.8 liters/min., respectively. More detailed heat transfer analyses will be performed as the design matures.

3.4 Thermal Bumpers

A major requirement of the vacuum vessel shells is that they be as transparent to electromagnetic radiation as possible in areas where they lie between the interaction point and any electromagnetic calorimetry. Because of this requirement relatively thin aluminum shells are used in these areas. Although designed to the intent of the ASME Pressure Vessel Code, these shells are necessarily thinner and have correspondingly higher deflections than those allowed for an ASME code stamped vessel. These deflections, which occur during the transition to a fully evacuated and cooled state are mitigated through the use of mechanical bumpers designed to transfer loads from the externally pressurized vacuum vessel to the internally pressurized cold liquid vessel. Heat transfer to the cold vessel through these bumpers can be minimized through the judicious use of insulating materials and standard thermal isolation design techniques. One initial concept uses a reentrant conical G10 cup attached to the vacuum shell in high deflection areas. The small end of the cup will contact the cold vessel wall as the two vessels deflect towards one another during the transition to operational conditions. One area of concern is that the relative motion of the vessel walls may subject the bumpers to shear loads. Design of the bumpers is in process and values for the heat transferred to the liquid vessel through the bumpers are not currently available. Future work will include detailed design and sizing of the bumpers which will depend on the as yet undetermined loading conditions.

A single design concept will be developed for both the barrel and end cap thermal bumpers. However, loads and thermal path lengths are expected to be slightly different for the two because of the greater surface areas of the end cap vessel heads and the location dependent size of the respective insulating vacuum spaces.

3.5 Super Insulation

Super insulation or Multilayer Insulation (MLI) is needed to intercept the high radiation heat load which would exist between the 300K vessel walls and the cryogenic liquid vessels (LAr at 87K, LKr at 120K). The minimum space available for MLI blanket installation is roughly 16mm (Figure 3.5-1). We have used this value in a worst case estimate of the heat load. Experience with MLI at the SSC is extensive and we recognize the potential variability in its effectiveness, which depends not only on the known

physical parameters, but also on the method of lay-up and any cracks or pinching which can occur at difficult locations. Even without consideration of such factors, we note that the reported average effective thermal conductivity of MLI in a high vacuum condition ($\leq 10^{-5}$ torr) may range from 1 to 8 $\times 10^{-8}$ W/mm K (for $\Delta T = 220$ K, i.e., 300-80K). Similarly, the measured heat flux coefficient can vary from 0.3 to 0.7 W/m^2.

Our estimates of the heat load are based on an assumed layer density of 22 layers/cm, although "optimum" values range from 20 to 30 layers/cm. For the 1.6 cm space available, there would be about 35 layers. Using two different formulas obtained from the literature, we calculated heat fluxes of 0.38 W/m^2 and 0.53 W/m^2. These calculations are consistent with experimental results for doubly aluminized mylar with glass fabric spacers, and they are in the range of heat flux data cited above. Therefore, we have conservatively used 0.5 W/m^2 to compute the heat loads onto all cryogenic vessel surface areas. The results are given in Tables 2.1-3 and 2.2-2 as the vessel shell entries for 1×10^{-6} torr. Entries given for the case of insulation vacuum degradation at 1×10^{-4} torr indicate an <u>estimated</u> 40% increase in heat load due to the resulting soft inter layer vacuum. We note that there is considerable scatter in the reported heat flux data for pressures between 10^{-5} and 10^{-2} torr. The "no vacuum" heat flux values were computed assuming that the insulating vacuum space was catastrophically ruptured and subsequently filled with dry GN_2 at one atmosphere to prevent icing. An average value of the GN_2 thermal conductivity in the temperature range 77K to 300K was used, and ice buildup was neglected.

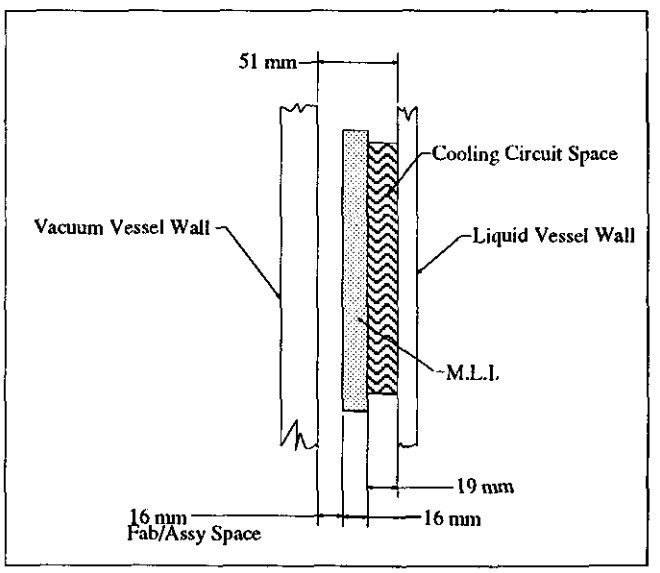

Figure 3.5-1 Stackup of Minimum Allocated Space for the Placement of MLI.

4.0 CONTROL AND MONITORING SYSTEM

4.1 Temperature Sensors

For the range of temperature 85 K < T < 300 K and accuracy's of 1%, it is recommended that four wire measurements be made using Platinum Resistance Thermometers (PRTs) rather than thermistors. Today inexpensive ($25) and accurate (< 0.5%) film type PRTs are available in a variety of ice-point resistance's. Accurate measurements will be required at critical locations, for example, on the HX tubing and adjacent preamplifier packages in the Outer EM where the heat loads are largest and the temperature uniformity most difficult to achieve. In this case it would be advisable to monitor temperatures at three locations along the length of the HX tubing in each octant (inlet, u-bend, and outlet) to ensure that design performance ΔTs are met. The mass flow rates of LAr can be adjusted as required by automatically controlled flow valves using the temperature inputs. Similarly, temperature measurements on other HX lines (inlet and outlet locations) should be compared to the LKr temperature at nearby locations and at various random locations within the vessel. Combined within pressure measurements at the same locations, these data will permit the LKr density to be calculated accurately to ensure conformity with the 1% maximum variation specification. Temperature measurements of the LAr coolant can be made on the outside surfaces of the inlet and outlet tubing within the insulating vacuum space.

4.2 Automatic Valves

Automatic valves suitable for long-term cryogenic service will be required in the cooling circuits to ensure that flow rates are maintained at the required levels. These valves must operate as key components in feedback loops with temperature sensors and flow metering instrumentation.

4.3 Pressure Monitors

Cryogenic pressure measurements are more difficult than temperature measurements. Two types of pressure transducers which have been used successfully at cryogenic temperatures as low as 2 K are strain-type sensors (e.g., Siemens) and variable reluctance transducers of the welded diaphragm type. Strain-type transducers are relatively inexpensive but they require sensitivity and zero offset corrections at cryogenic

temperatures. They are characteristically noisy but may have adequate resolution for this application. They have the advantage of small size and can be conveniently mounted in confined locations. The much larger variable reluctance transducers are more accurate, more expensive, and available for measurement of a wide range of absolute or differential pressure. Their size limits installation flexibility, but the diaphragm assembly itself can be fully immersed in the cryogen. One possibility is to use both types of transducers at certain locations, where the variable reluctance type can be used to verify calibration of the strain-type sensor. Various other pressure measuring devices will be required to monitor pump performance on the lines external to the calorimeter.

4.4 Flow Control and Monitoring

Flow metering will be required in each section cooling circuit to ensure that flow rates are maintained at levels which are consistent with section heat loads. Accurate cryogenic flow meters have been made using variable reluctance differential pressure transducers in conjunction with suitably sized orifice plates in external flow lines. Flow monitoring of individual HX lines is not required, provided that adequate temperature measurements are made as described in Section 4.1.

5.0 FUTURE WORK

5.1 System Reliability Trades

System reliability trade studies will be performed to determine the optimum level of redundant manifolding. These studies will take into account the gain in reliability afforded by multiple redundant supply and return manifolds versus the reliability penalties accrued from the addition of feedthroughs, valves, and bi-metallic joints.

5.2 Three Dimensional Thermal Fluid Analysis

Some preliminary analyses based on correlation's (Appendix A) and 2 dimensional analytical modeling (Ref. 7) have been performed to assess performance of the barrel heat exchangers. As the design matures analyses will incorporate three dimensional modeling

to better understand the level of convective interaction between the submerged calorimeter electronics and the cooling system heat exchangers for all orientations. Coupled fluid thermal models will also be employed both to optimize the various heat exchanger systems and to model system operation under operational and emergency conditions. These analyses will ultimately support system validation with respect to the operational performance requirements. Computer models based on detailed engineering designs will also be used to verify the various system heat loads such as the vessel supports, cable feedthroughs, piping feedthroughs, thermal bumpers and radiative loads from the vacuum vessel.

5.3 Thermo-Structural Analysis

High fidelity two and three dimensional linear and nonlinear thermo-structural analyses will be performed to model the effects of relative motion between components due to non uniform thermal expansion and contraction during system cool down, warm-up, and long term operation. In particular, the performance of the thermal bumpers during system cool down will be analyzed including shear loads due to friction between the bumpers and vessel walls.

5.4 Piping Feedthrough Design

It is important to ensure that critical feedthroughs will be reasonably accessible for repair or replacement without requiring major breaches of the cryostats. Therefore, designs will be optimized for reliability, assembly, and maintenance. One of the more critical areas of cryostat penetration/feedthrough design is the incorporation of bi-metallic joints to make the transition from aluminum cryostat vessels to stainless steel bellows. Reliability concerns are high for these types of transition joints and designs will have to be assessed for their life cycle survivability over the lifetime of the system. Piping feedthroughs will also incorporate design features which will minimize heat leakage into the cryostats and limit stress on lines during thermal cycling. Wherever possible feedthrough bellows will be placed such that a positive external pressure is present to minimize squirm.

Achievement of these design goals is challenging in view of the physical space limitations within the cryostats.

6.0 REFERENCES

GEM Papers

1. "GEM Technical Design Report", GEM-TN-93-262, (April 30, 1993).
2. "GEM Calorimeter Barrel Electromagnetic Structure", GEM-TN-93-321, (1993).
3. "The DØ Revised Design Report", DØ Note 512, Fermilab, (1985).
4. "Design Description of The GEM Barrel Calorimeter Cryostat", GEM-TN-93-313, (1993)
5. "GEM Calorimeter Feedthrough Design", GEM-TN-93-315.
6. "Selected Cryogenic Data Notebook", Volume I, page VII-B-4, BNL 10200R, (August 1980).
7. J. Krupczack and A. Sidi-Yekhlef, "A Two Dimensional Thermal/Fluid Model of the GEM Barrel Electromagnetic Calorimeter", To Be Published as a GEM Technical Note for the SSCL.
8. Structure of the GEM End Cap Electromagnetic Calorimeter Structure, GEM-TN-93-321, (1993).

Heat Transfer/Fluid Dynamics

9. A.P. Fraas, Heat Exchanger Design, 2nd edition, John Wiley & Sons, New York, 1989, Chapters 4,8, & 12.

10. J.P. Holman, Heat Transfer, 4th Edition, McGraw-Hill, New York, 1976, Chapters 7, & 10.

11. F.P. Incropera and D.P. DeWitt, Fundamentals of Heat transfer, John Wiley & Sons, New York, 1981, Chapter 9.

12. G.K. White, Experimental Techniques in Low Temperature Physics, 3rd edition Clarendon Press, Oxford, 1979; Chapter III.

13. S. W. Churchhill and H.H.S. Chu, Int. J. Heat Mass Transfer 18, 1049 (1975).

14. J. G. Knudson and D.L. Katz, Fluid Dynamics and Heat Transfer, McGraw-Hill, New York, 1958, Part III.

15. NBS Monograph 131, Thermal Conductivity of Solids at Room Temp. and Below, Figure 43b, p. 292.

16. Castle Metals, Chicago, Product Catalog (1984).

Fluid Properties

17. Encyclopedia of Chemical Technology, Vol. 12, "Helium Group Gases", Table 4, p.254.

18. Al Jaques, "Thermophysical Properties of Argon", TM-1517-A.

19. V.A. Rabinovich et.al., "Thermophysical Properties of Neon, Argon, Krypton, and Xenon," Hemisphere Press (?), 1988, pp.436-506.

Multi Layer Insulation

20. G.M. York, ICEC 12, 172 (1988).

21. T. Amand *et.al.*, ICEC 12, 162 (1988).

22. S.L. Bapat *et.al.*, Cryogenics 30, 700 (1990).

23. S.L. Bapat *et.al.*, Cryogenics 30, 711 (1990).

24. H. Burmeister *et.al.*, Adv. Cryo. Eng. 33, 313.

25. "NRC-2 Super insulation: Metallized Products, inc., Specification Sheets.

26. Q.S. Shu *et.al.*, Adv. Cryo. Eng. 31, 455 (1985).

27. Q.S. Shu *et.al.*, Cryo. 26, 671 (1986).

28. T. Ohmori *et.al.*, Adv. Cryo Eng. 33, 323 (1987).

29. M. Taneda *et.al.*, Adv. Cryo Eng. 33, 305 (1987).

30. W. Barth *et.al.*, Cryo. 28, 607 (1988).

APPENDIX A

Heat Transfer Analysis for Barrel Outer EM Heat Exchanger

Heat Transfer Analysis for Barrel Outer EM Heat Exchanger

$\frac{1}{2}$ EM:

$\dot{Q}$Load = 1.92 kW (1920 preamps @ 0.1 W ea.)

Coolant: L Argon @ 118 K and ~ 149 PSI (saturated)

Cryostat: L Krypton @ 120 K and ~44 to 55 PSI (subcooled)

Properties Used -- (SI units used throughout this analysis)

				@ ~120 K		
		LAr	LKr	304 SS	Cu	6063 Al
β	Volume Expansivity	7.1×10^{-3} K^{-1}	3.31×10^{-3} (calculated)			
ρ	Density	1176 kg/m^3	~2420			
c_p	Specific Heat	1298 J/kg K	535			
η	Viscosity	1.17×10^{-4} Pa-S	4.31×10^{-4}			
λ	Thermal Cond.	8.66×10^{-2} W/m-K	9.05×10^{-2}	10	410	205
Pr ($=c_p\eta/\lambda$)	Prandtl #	1.77 —	2.55 (Calculated)			
		Ref. = A1 Jaques, "Thermo. Ppties of Argon" TM-1517-A	Ref. = Encylo. of Chem. Tech, Table 4, Vol. 12, "Helium Group Gases", p. 254			

Approach: 1) Determine the minimum required mass flow rate of LAr to provide cooling based on the known heat load from preamps. 2) Use a single formula for the overall heat transfer between the liquid coolant, flowing through tubing, and a surrounding liquid bath (LKr), along with the appropriate heat transfer correlation formulas, to determine the required geometries of the cooling system plumbing, section by section. Determine flow regimes and pressure drops. Modify the plumbing geometry and mass flow rates as required to obtain acceptable heat exchanger (HX) performance.

Define a "figure-of-merit" function $f = \Delta T_{out}/\Delta T_{in}$

$$① \quad f = f(\dot{M}) = \exp\left\{-\pi L / \dot{M} c_p \left(\frac{1}{h_{Ar} D_1} + \frac{\ln(D_2/D_1)}{2\lambda_{\substack{tube\\wall}}} + \frac{\ln(D_3/D_2)}{2\lambda_{\substack{insul.\\sleeve}}} + \frac{1}{h_{Kr} D_3} \right)\right\}$$

Ref. = G.K. White, Chapter III
Experimental Techniques in Low Temperature Physics (1979)

$\dot{M}$	=	total mass flow rate	D_1	=	tube I.D.
$\dot{m}$	=	subdivided mass flow rate	D_2	=	tube O.D.
L	=	length of a given section	D_3	=	insulation sleeve OD, where used
c_p	=	specific heat of coolant			
h	=	heat transfer coefficient			
λ	=	thermal conductivity			

$$\neq \quad \dot{Q} = \dot{M}\, c_p\, \Delta T_{out} = \dot{M}\, c_p\, f\left(\dot{M}\right)\Delta T_{in} \qquad ; \quad \text{let } \Delta T_{in} = 2K$$

$$\Rightarrow \dot{M}\, f\left(\dot{M}\right) = \dot{Q} \,/\, c_p\, \Delta T_{in} = 1.92 \times 10^3 W / 1298 \frac{J}{kg\,K} \cdot 2K = 0.740\ kg/s$$

Since $f \rightarrow 1$ is the <u>ideal</u> case for the inlet tubing, we need $\dot{m}$ to scale with the heat load requirement of any subsection of the EM.

A system simplification for the inlet tubing would be to take advantage of the poor thermal conductivity of 304 SS, i.e., use a wall thickness which might provide a sufficiently high thermal resistance without recourse to G-10 or other insulation material or sleeving.

A. Inlet Tube (one of four short stainless steel tubes which distribute $\dot{M}/4$ to a set of four stainless steel header tubes and their associated connections to the Cu HX tubes)

$$\left.\begin{array}{l} D_1 = 0.370'' = 9.40 \times 10^{-3}\ m \\ D_2 = 1/2'' = 1.27 \times 10^{-2}\ m \\ D_3 = D_2 \text{ (no G-10 sleeve)} \end{array}\right\} \begin{array}{l} 0.065'' \text{ wall} \\ = \text{candidate values} \end{array}$$

L = 0.10 m (this is the ~ length from the EM vessel wall to any one of four headers, forming 4 x 90° arcs. Then the flow rate in the inlet is:

$$\dot{m}_{inlet} = \frac{\dot{M}}{4} \text{ and Eqn. ① in SI Units becomes:}$$

$$f = \exp\left\{-4\pi\,(0.10)/\dot{M}\,(1298) \times \left(\frac{1}{h_{Ar}D_1} + \frac{\ln\left(D_2/D_1\right)}{2\lambda_{ss}} + \frac{1}{h_{Kr}D_2}\right)\right\}$$

Determine if flow in the 9.40×10^{-3}m I.D. is "fully turbulent":

$$N_R = 4\dot{m} \,/\, \pi\eta D_1 = \frac{4\dot{M}}{4} \,/\, \pi\left(1.17 \times 10^{-4}\right)\left(9.40 \times 10^{-3}\right)$$

We want:

$$N_R \approx 6 \times 10^3 \leq 2.894 \times 10^5 \dot{M} \Rightarrow \dot{M} \geq 2.07 \times 10^{-2} \text{ kg/s}$$

so that for the range of mass flow rate needed here, the flow is fully turbulent, and $N_R \geq 2.1 \times 10^5$ (Blasius regime)

(Laminar flow in the inlet tube would be preferable for poor heat transfer, but it cannot be achieved for practical D_1 and $\dot{M}$).

$$\text{Evaluate} \left(\frac{1}{h_{Ar} D_1} + \frac{\ln (D_2 / D_1)}{2\lambda_{ss}} + \frac{1}{h_{Kr} D_2} \right)$$

1st term: for the Argon coolant in turbulent flow,

$$Nu = 0.023\, N_R^{0.8}\, Pr^{0.4} \text{ (coolant warming)}$$

$$h_{Ar} D_1 = \lambda_{Ar}\, Nu$$

$$= \lambda_{Ar}\, 0.023\, (4\dot{M}/4\, \pi\eta D_1)^{0.8}\, Pr^{0.4}$$

$$= (8.66 \times 10^{-2})\, (0.023)\, (\dot{M}/(1.17 \times 10^{-4})\, \pi\, D_1)^{0.8}\, (1.77)^{0.4}$$

$$= 1.40 \left(\frac{\dot{M}}{D_1} \right)^{0.8}$$

Then:

$$1/h_{Ar} D_1 = 0.714\, D_1^{0.8}\, \dot{M}^{-0.8}$$

For $D_1 = 9.4 \times 10^{-3}$ m and $\dot{M} = 0.80$ kg/s, the min. flow rate,

$$1/h_{Ar} D_1 = \boxed{2.97 \times 10^{-2} \text{ mK/W}}$$

2nd term: for the SS tube itself, having $D_2 = 1.27 \times 10^{-2}$ m,

$$\frac{\ln\left(D_2/D_1\right)}{2\lambda_{ss}} = \frac{\ln\left(1.27/0.94\right)}{2(10)} = \boxed{1.50 \times 10^{-2} \text{ mK/W}}$$

(Note that this value $\Rightarrow$ the SS wall provides about 35% more impedance to heat transfer than the flowing LAr).

3rd term: For the heat transfer via free convection through the relatively stagnant krypton bath in the unconfined locations of the four inlet tubes (actually, 2 inlets are mostly horizontal, 2 mostly vertical), consider the inlet as a horizontal cylinder, for which the correlation Nu # is a fairly complicated function given by Churchill and Chu:

a) $\overline{N}_u = \left\{0.60 + 0.387 R_{a_D}^{1/6} / \left[1 + (0.559/P_r)^{9/16}\right]^{8/27}\right\}^2$

A simpler version is:

b) $\overline{N}_u = C R_{a_D}^n$, $C = 0.125$ and $n = 0.333$ for $10^7 < R_{a_D} < 10^{12}$

where:

$R_{a_D} = g\beta\Delta T D_2^3 / \upsilon\alpha$; let $\Delta T = 120 - 118$ K $= 2$ K

$\left.\begin{array}{l}\upsilon = \text{kinematic viscosity} \\ \alpha = \text{thermal diffusivity}\end{array}\right\} \alpha\upsilon = \lambda\eta / p^2 c_p$

$\alpha\upsilon = (9.05\times10^{-2})(4.31\times10^{-4})/(2420)^2(535) = 1.245\times10^{-14}$

Then:

$R_{a_D} = (9.8)(3.31\times10^{-3})(2)(1.27\times10^{-2})^3 / 1.245\times10^{-14}$

$= \boxed{1.07\times10^7}$

a) $\overline{N}_u = \left\{0.60 + 0.387(1.07\times10^7)^{1/6} / \left[1 + (0.559/2.55)^{9/16}\right]^{8/27}\right\}^2$

$= \boxed{33.2}$

or

b) $\overline{N}_u = 0.125(1.07\times10^7)^{0.333} = \boxed{27.4}$

Use the larger $\overline{N}_u$ value as a worst case:

$1/h_{k_r} D_2 = 1/\lambda_{k_r} N_u = 1/(9.05\times10^{-2})(33.2) = \boxed{3.33\times10^{-1}\ \text{mK/W}}$

Therefore, the krypton bath itself provides the greatest impedance to heat transfer to the LAr flowing in the inlet tube. Calculate the temperature rise of the LAr along the inlet length:

$f = \exp\left\{-4\pi(0.10)/(0.8)(1298)(2.04\times10^{-2} + 1.50\times10^{-2} + 3.33\times10^{-1})\right\}$

$f = \exp(-3.28 \times 10^{-2}) = 0.997$

$\Rightarrow \Delta T_{out} = 0.981\,\Delta T_{in} = 0.967(2K) = 1.99K$

$\Rightarrow$ The LAr warms by only ~ 0.01K along this inlet section if the total 1/2 EM mass flow rate is 0.8 kg/s.

Two assumptions in this analysis are:

1) Free convection from a horizontal cylinder.

2) $\Delta T = 2$ K to compute R_{a_d} (an exact solution for ΔT could have been found, assuming slow laminar flow of the LKr in the vicinity of the header assembly).

Pressure drop in the inlet tube:

③ $$\Delta P = 0.2414 \left[\frac{\eta \dot{M}^7}{D_1^{19}}\right]^{1/4} \frac{L}{\rho} \qquad \text{(Blasius Regime)}$$

where:

$$\dot{m} = \dot{M}/4 = 0.8/4 = 0.20 \text{ kg/s}$$

$$\Delta P = 0.2414 \left[\frac{(1.17\times10^{-4})(0.20)^7}{(9.4\times10^{-3})^{19}}\right]^{1/4} \frac{0.10}{1176} = 3.20\times10^3 \text{ Pa}$$

$$\Delta P = \frac{3.20\times10^3 \text{ Pa}}{6895 \text{ Pa/PSI}} = \boxed{0.08 \text{ PSI}}$$

B. Inlet Manifold Section (One of four, each having an arc length of ~ 2.8 m and 10 connections to 28 cm long tubes which join 10 equally spaced Cu HX tubes).

Use the same tube size as inlet tube to eliminate the need for additional fittings.

Use equations ① and ③ above.

The divided flow in this section is such that the full $\dot{M}/4$ is decreased by $\dot{M}/40$ as it passes each Cu HX tube. The total pressure drop across the 2.8 m header is only 0.77 PSI.

The two values of f in each 28 cm section of the header and the complementary 28 cm feeder tube have been calculated to determine the heat gain up to each Cu tube inlet. Typically, these values differ because of the different mass flow rates involved, and the pair products give values of $f \approx 0.97$ ranging from 0.90 at the first inlet to 0.83 at the tenth inlet, due to heat gain at low mass flow rates. Therefore, the available ΔT is diminished by ~10% (first inlet) to ~17% (tenth inlet).

C. Heat Exchanger Tubing -- See below, Page 8.

D. Outlet Manifold Section -- (One of four).

The recommended cross-sectional area for the outlet manifold, to ensure even flow distribution through the HX tubing, for an "inclined" HX matrix, is given in Reference 9 as:

$$A_{out} = A_{in} \ / 0.636$$

$$= 6.94 \times 10^{-5}\ m^2 / 0.636 = 1.091 \times 10^{-4}\ m^2$$

It would seem prudent to incorporate this idea which can be easily implemented by a change in tube wall thickness.

Then:

$$\frac{D_{1_{out}}}{D_{1_{in}}} = \left(\frac{1}{0.636}\right)^{1/2} = 1.254$$

$$D_{1_{out}} = 1.254 \times 0.37'' = 0.464''$$

$$1/2''\ OD \Rightarrow wall = 0.018''$$

Assume 1/2" x 0.020" wall SS tubing

$$D_2 = 1.27 \times 10^{-2}\ m$$

$$D_1 = 0.46'' = 1.17 \times 10^{-2}\ m$$

The pressure drop across the outlet header is estimated to be 0.30 PSI. Heat gain here should be minimal since the ΔT is small.

E. Outlet tube

- length $\approx$ 0.10 m
- assume same tube sizing as in D above to eliminate the need for additional fittings

Then:

$$\frac{\ln\left(D_2/D_1\right)}{2\lambda_{ss}} = \frac{\ln\left(1.27/1.17\right)}{20} = \boxed{4.1\times10^{-3}\ mK/W}$$

This is about 7x less thermal impedance than the flowing LAr, but the heat transfer is still dominated by natural convection in the LKr.

$$\Delta P = 0.2414\left[(1.17\times10^{-4})(0.20)^7 / (1.17\times10^{-2})^{19}\right]^{1/4} 0.10/1176 = 192 \text{ Pa}$$

$$= \boxed{0.03 \text{ PSI}}$$

C. <u>Heat Exchanger Tubing</u> - For even flow distribution in the 10 HX tubes, it is recommended that the matrix static pressure drop exceed the inlet head pressure by at least a factor of 2. The LAr (pressurized at ~149 PSI) is further elevated by about 40 psi by pumps, to provide an estimated 20 psi, after other system losses, to ensure this.

$$2P_H = 2 \text{ x Inlet head pressure} = \rho V^2$$

$$= \dot{m}^2 / \rho A^2$$

Where:

$$\dot{m} = \dot{M}/4 \quad , \quad A = \pi D_1^2 / 4$$

Then:

$$2P_H = \left(\frac{\dot{M}}{4}\right)^2 \Big/ \rho \left(\frac{\pi D_1^2}{4}\right)^2 = \left(\frac{\dot{M}}{\pi D_1^2}\right)^2 \frac{1}{\rho}$$

$$= \left(\frac{0.8}{\pi(9.4\times10^{-3})^2}\right)^2 \frac{1}{1176} = 7.06\times10^3 \text{ Pa}$$

$$2P_H = \boxed{1.0 \text{ PSI}}$$

Since LAr is a dense fluid, the inlet pressure at the lowermost HX tube will be higher than the uppermost, for any arc, by

$$\Delta P_{\text{Hydrostatic}} = \rho g \Delta h = \rho g R$$

$$= (1176)(9.8)(1.95)$$

$$= 2.25 \times 10^4 \text{ Pa} = \boxed{3.26 \text{ PSI}}$$

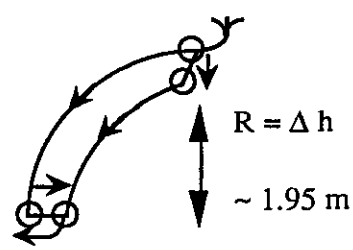

This means that the steady state pressure drop across any HX tube should probably be >3.3 PSI to ensure even flow, although the cooling system is closed.

Candidate HX tubing material --- ETP Cu or equivalent but <u>not</u> phosphorous deoxidized Cu. A possible source is Castle Metals, ASTM B280/CDA 122 - refrig. service (ASTM B75/CDA 122 probably ok).

3/16"OD x .030" wall

$D_2 = 0.1875" = 4.76 \times 10^{-3}$ m

$D_1 = 0.1275" = 3.24 \times 10^{-3}$ m

$L = 4$ m

$\dot{m} = \dot{M}/40 = 0.8/40 = 0.02$ kg/s

$$N_R = 4\dot{m}/\pi\eta D_1 = \dot{M}/10\pi\eta D_1$$
$$= 0.8/10\pi(1.17 \times 10^{-4})(3.24 \times 10^{-3})$$
$$= \boxed{6.7\text{x}10^4} \quad \text{turbulent, Blasius regime}$$

$$\Delta P = 0.2414\left[\frac{\eta\dot{M}^7}{D_1^{19}}\right]^{1/4}\frac{L}{\rho}$$

$$= 0.2414\left[\frac{(1.17 \times 10^{-4})(2.0 \times 10^{-2})^7}{(3.24 \times 10^{-3})^{19}}\right]^{1/4}\frac{4}{1176}$$

$$= 6.07 \times 10^4 \text{ Pa} = \boxed{8.8\text{PSI}}$$

which is greater than $\Delta P_{Hydrostatic}$ or ρV^2

This ΔP value is sufficiently high to ensure an even flow distribution in the 10 HX tubes and still allows for a ΔP cushion of about 10 PSI (to be dropped across an external throttling value) in the case that a larger $\dot{m}$ is required.

But because of the small O.D., more surface area in contact with the LKr is required.

Tubing spacing is ~ 12 cm. One solution is to employ a thin Cu plate across each U HX tube, as discussed below.

We now want $f \rightarrow 0$, i.e., $\Delta T_{out} \approx 0$, such that the LAr passing through any HX tube absorbs all of the module preamp heat load (1.92 KW/40 = 48 W) and exits the tubing at ~120K.

$$f = \exp\left\{-\pi L/\dot{M}c_p\left(\frac{1}{h_{Ar}D_1} + \frac{\ln(D_2/D_1)}{2\lambda_{ss}} + \frac{1}{h_{Kr}D_2'}\right)\right\}$$

where D_2' represents the enhanced surface area, and

$$D_2' \approx 12\text{ cm} + 2\pi D_2 = 15\text{ cm} = 1.5 \times 10^{-1}\text{ m}$$

The Cu plate must be thick enough to transfer some fraction of the 48 W between the 2 tube "sections", with minimal ΔT, i.e., provide a thermal short in the transverse direction. The plate will help produce a more evenly cooled "LKr layer"; it can be perforated to allow for convection, and the degree of perforation can vary along the 2m length to vary the "transverse" conductance. Since both sides of the plate are involved, the reduced HX effective length (2m) is offset, so that D_2' remains ~15 cm.

$$f = \exp\{-\pi 4/(0.02)(1298)(\text{as above})\}$$

$$= \exp\{-0.484/(\text{as above})\}$$

1st term:

$$h_{Ar}D_1 = \lambda\, Nu$$

$$= (8.66 \times 10^{-2})\,(0.023)\,[4(0.02)/\pi(1.17\times10^{-4})(3.24\times10^{-3})]^{0.8} \times (1.77)^{0.4}$$

$$= (8.66 \times 10^{-2})\,(210)$$

$$= 18.2$$

$$\frac{1}{h_{Ar}D_1} = \boxed{5.49\times10^{-2}\text{ mK/W}}$$

2nd term:

$$\frac{\ln\left(D_2/D_1\right)}{2\lambda_{cu}} = \frac{\ln\left(4.76/3.24\right)}{2(410)} = \boxed{4.7\times10^{-4}\text{ mK/W}}$$

(Negligible thermal resistance across Cu tube wall)

3rd term:

Model the heat transfer between the CU plate/tubing and LKr using a correlation for concentric cylinders, because of the confined space at preamp module locations (D_{out}, D_{in} = diameters).

$$\frac{\dot{Q}}{L} = 2\pi\lambda_{eff}\,\Delta T/\ln(D_{out}/D_{in}) = \frac{h_{Kr}A\,\Delta T}{L}$$

$$A \sim \pi\frac{(D_{out}+D_{in})}{2}L \Rightarrow \frac{h_{Kr}A\Delta T}{L} = \frac{h\pi(D_{out}+D_{in})\Delta T}{2}$$

$$\Rightarrow \; h_{Kr} = 4\lambda_{eff} / (D_{out} + D_{in}) \ln (D_{out} / D_{in})$$

where:

$$\lambda_{eff} = \lambda(0.386)[Pr/(0.861+Pr)]^{1/4} \overset{*}{Ra}_c^{1/4}$$

$$\overset{*}{Ra}_c = \left[\ln\left(D_{out}/D_{in}\right)\right]^4 Ra_L \Big/ (D_{out} - D_{in})^3 \left(D_{in}^{-0.6} + D_{out}^{-0.6}\right)^5$$

where:

$$Ra_L = g\beta\Delta T(D_{out} - D_{in})^3 / \upsilon\alpha$$

$$\Rightarrow \; \overset{*}{Ra}_c \; \frac{\left[\ln\left(D_{out}/D_{in}\right)\right]^4 g\beta\Delta T}{\upsilon\alpha(D_{in}^{-0.6} + D_{out}^{-0.6})^5}$$

The spacing between plate and preamp is ~ 2 cm. Take $\Delta T \approx 2.0$ K for the calculation.

$$R_{out} \sim 1.61 \text{ m} \rightarrow D_{out} = 3.22\text{m}$$

$$R_{in} \sim 1.59 \text{ m} \rightarrow D_{in} = 3.18\text{m}$$

$$\overset{*}{Ra}_c = \frac{\left[\ln\left(322/318\right)\right]^4 (9.8)\left(3.31 \times 10^{-3}\right)(2.0)}{\left(1.245 \times 10^{-14}\right)\left(3.18^{-0.6} + 3.22^{-0.6}\right)^5}$$

$$= \boxed{1.30\text{x}10^5}$$

Then:

$$\lambda_{eff} = \left(9.05 \times 10^{-2}\right)(0.386)\left[2.55/(.861 + 2.55)\right]^{1/4}\left(1.30 \times 10^5\right)^{1/4}$$

$$= \left(9.05 \times 10^{-2}\right)(6.82)$$

$$= \boxed{0.617}$$

$$h_{Kr} = 4\,\lambda_{eff} / \left(D_{out} + D_{in}\right) \ln\left(D_{out}/D_{in}\right)$$

$$= 4\,(0.617)/(3.22 + 3.18) \ln (3.22/3.18)$$

$= 31\ W/m^2K$ We note that John Krupczak's 2D thermal model (FLUENT) at the SSCL gives $h_{Kr} = 68\ W/m^2K$ over a full quadrant comprising 10 preamplifiers and 10 HX pairs. (See text).

$$h_{Kr}D_2' = 31 \times 1.5 \times 10^{-1} = 4.65$$

$$1/h_{Kr}D_2' = \boxed{2.15 \times 10^{-1}\ mK/W}$$

Then:

$$f = \exp\left\{-0.484/\left(5.49 \times 10^{-2} + 4.7 \times 10^{-4} + 2.15 \times 10^{-1}\right)\right\}$$

$\boxed{f = 0.17}$ This is a fairly good result.

$\Rightarrow \sim 83\%$ of the available temperature difference is used in the HX tubing.

We note that if two Cu plates were used, the effective surface dimension D_2' would be doubled and $1/h_{Kr}D_2'$ would become 0.107, for which $f = 0.05$ and 95% of the ΔT would be used.

Calculate the $\Delta T_\perp$ between the LAr (at tube axis) and the tube wall. Consider the case of no Cu plates and constant heat flux into the 4 m long Cu tube.

$$\Delta T_\perp = \dot{m}\ c_p f\ \Delta T_{in} / \lambda\ Nu\ L$$

$$= (0.02)\ (1298)\ (0.95)\ (2) / (8.66 \times 10^{-2})\ (210)\ (4)$$

$$= \boxed{0.67\ K}$$

This $\Delta T_\perp$ would be less if the Nu were larger (i.e., smaller D_1 or larger $\dot{m}$). Since ΔP which $\sim D_1^{-19/4}$ would exceed the allowable 20 psi for the next smallest available tube size (1/8" x 0.030" wall), the better option is a slightly larger $\dot{m}$.

Calculate the estimated ΔT between preamps and HX. Assume that the forty Cu plate/tube pairs provide a nearly continuous circle at the 1.6 m radius.

$$\frac{\dot{Q}}{A} = \frac{1.92 \times 10^3 W}{\pi DL} = \frac{1.92 \times 10^3 W}{\pi\ (3.2m)\ (2m)} = 95\ \frac{W}{m^2} \qquad \text{(average heat flux)}$$

Then for $h_{Kr} = 31\ W/m^2K$

$$\Delta T = \dot{Q} / Ah_{Kr} = 95\frac{W}{m^2} / 31\frac{W}{m^2K} = \boxed{3.0K}$$

Conclusions:

Because of the inlet header losses (about 13%) and the non ideal heat transfer of the HX system, the inlet temperature of the LAr coolant should be colder than the 120 K LKr bath by about 3.5 K (i.e., at 116.5 K) to realize a 2 K temperature rise within the HX. A slightly higher mass flow rate ($\dot{M} \approx 1.0$ kg/sec), with ΔP higher by about 38%, would ensure lower refrigeration losses and, therefore, allow a higher LAr inlet temperature (>117 K). The HX ΔP would be about 12 psi if $\dot{M} = 1.0$ kg/sec.